

A parametrix method for elliptic surface PDEs

Tristan Goodwill¹
Department of Statistics
University of Chicago
Chicago, IL 60637
tgoodwill@uchicago.edu

Michael O'Neil²
Courant Institute, NYU
New York, NY 10012
oneil@cims.nyu.edu

January 24, 2024

¹Research supported in part by the Research Training Group in Modeling and Simulation funded by the National Science Foundation via grant RTG/DMS-1646339, by the Simons Foundation/SFARI (560651, AB), and the Office of Naval Research under awards #N00014-18-1-2307 and #N00014-21-1-2383.

²Research supported in part by the Simons Foundation/SFARI (560651, AB) and the Office of Naval Research under awards #N00014-18-1-2307 and #N00014-21-1-2383.

Abstract

Elliptic problems along smooth surfaces embedded in three dimensions occur in thin-membrane mechanics, electromagnetics (harmonic vector fields), and computational geometry. In this work, we present a parametrix-based integral equation method applicable to several forms of variable coefficient surface elliptic problems. Via the use of an approximate Green's function, the surface PDEs are transformed into well-conditioned integral equations. We demonstrate high-order numerical examples of this method applied to problems on general surfaces using a variant of the fast multipole method based on smooth interpolation properties of the kernel. Lastly, we discuss extensions of the method to surfaces with boundaries.

Keywords: Surface elliptic PDE, Laplace-Beltrami, parametrix, surface boundary value problems

Contents

1	Introduction	2
2	Analytical preliminaries	4
2.1	Parametrix basics	4
2.2	Surface basics	5
2.3	Existence and uniqueness for the Laplace-Beltrami problem	5
3	A parametrix for the Laplace-Beltrami problem	6
4	Elliptic PDEs on surfaces	11
4.1	Existence of solutions	11
4.2	Elliptic problems without advection	14
4.3	Elliptic problems with advection	18
5	Elliptic boundary value problems on surfaces	19
5.1	Existence of solutions	19
5.2	Neumann boundary conditions	21
5.3	Dirichlet boundary conditions	25
6	A numerical solver	27
6.1	Nyström discretization	27
6.1.1	Singular quadrature	27
6.1.2	Nearly singular quadrature	28
6.1.3	Smooth quadrature	31
6.1.4	Edge quadrature	31
6.2	Fast matrix vector multiplication	31
7	Numerical Experiments	33
7.1	Spherical harmonic validation	34
7.2	A Laplace-Beltrami problem	34
7.3	A Helmholtz-Beltrami problem	35
7.4	A variable coefficient surface PDE	37
7.5	Boundary value problems	37
8	Conclusion	38

1 Introduction

For most of the constant-coefficient (elliptic) partial differential equations (PDEs) of classical mathematical physics, exact forms of the solution operator, or Green's function, are widely known and often used to transform boundary value problems into boundary integral equation formulations. In many situations, the resulting integral equations are the preferred formulation for solving the problem numerically due to their conditioning properties and their ease of handling complex geometries (including unbounded ones). As a result of incredible development over the past 20-30 years in areas such as hierarchical linear algebra, fast multipole methods, quadrature for singular functions, and computational geometry, obtaining high-order accurate solutions of PDEs via integral equation formulations is becoming more and more commonplace.

However, for the majority of PDEs, which are in general not constant-coefficient, the associated analytical and numerical machinery is virtually non-existent due to the absence of known Green's functions (and even ones that are known present difficulties, due to their non-translational-invariance). Almost all numerical approaches rely on a direct discretization of the differential operator via finite elements or finite difference schemes. However, often times an *approximate* Green's function, also known as a parametrix, can be constructed that can transform the PDE into an integral equation, albeit with kernels that need not satisfy the underlying homogeneous PDE themselves. A particular class of such elliptic PDEs that are of interest are what we call *surface PDEs*.

Elliptic PDEs on a surface are an extension of the corresponding problems in the plane. To be more precise, we let Γ be a smooth closed surface embedded in \mathbb{R}^3 , and $\nabla_{\Gamma \cdot}$ and ∇_{Γ} be the intrinsic surface divergence and surface gradient on Γ . We then define an elliptic PDE along Γ to be one of the form

$$\nabla_{\Gamma} \cdot a \nabla_{\Gamma} u + \mathbf{b} \cdot \nabla_{\Gamma} u + cu = f. \quad (1.1)$$

Above, the goal is to find a function u given some known function f , some smooth and positive function a , some continuous tangential vector field \mathbf{b} , and some continuous function c . Our assumptions on these functions and the geometry will be made more explicit later on in the manuscript.

A particularly important surface elliptic problem is the Laplace-Beltrami problem, in which we wish to find a u such that

$$\Delta_{\Gamma} u := \nabla_{\Gamma} \cdot \nabla_{\Gamma} u = f. \quad (1.2)$$

The operator Δ_{Γ} is known as the Laplace-Beltrami operator and is the surface equivalent of the Laplace operator. The Laplace-Beltrami problem appears in many fields, including computer graphics for interpolation and shape analysis [3, 69], plasma physics [55], vesicle deformation in biological flows [66, 70], surface diffusion [5, 27], computational geometry [47], and computer vision [4]. It is also used in electromagnetics to find the Hodge decomposition of a tangential vector field into curl-free and divergence-free components. See Section [24, 25, 60, 62] for more details regarding such decompositions, their uses, and a proof of their uniqueness.

The Laplace-Beltrami problem is not the only equation of the form (1.1) that is of interest. For example, the oscillations of thin films [37, 38, 50] can be modeled by the Helmholtz-Beltrami problem:

$$(\Delta_{\Gamma} + k^2) u = f, \quad (1.3)$$

where k is a positive function that is typically constant. Another example that we shall mention occurs when attempting to solve the diffusion equation on a surface [20, 61] using the method of semi-discretization. The equation we consider is

$$\partial_t u = \Delta_{\Gamma} u, \quad (1.4)$$

where u represents some quantity diffusing over Γ . As an example, we suppose that we discretize (1.4) in time with the backwards Euler method:

$$\frac{u(t_{n+1}) - u(t_n)}{\Delta t} = \Delta_{\Gamma} u(t_{n+1}), \quad (1.5)$$

where $\Delta t = t_{n+1} - t_n$. Rearranging this equation results in a modified Helmholtz-Beltrami problem for the solution at the next timestep, $u(t_{n+1})$:

$$\Delta_\Gamma u(t_{n+1}) - \frac{1}{\Delta t} u(t_{n+1}) = -\frac{1}{\Delta t} u(t_n). \quad (1.6)$$

If the diffusion equation is complicated by varying the diffusion constant or adding a drift term, such as is considered in [59], the analogous elliptic equation has a non-constant a or non-zero \mathbf{b} .

There are a few existing numerical schemes for solving surface elliptic problems. Many methods are based on direct discretization of the differential operators, including finite element methods [5, 9, 10, 13, 14, 21, 22], the so-called *virtual element method* [6, 33], differencing methods [72], pseudo-spectral methods [44], and hierarchical Poincaré–Steklov methods [30]. These schemes all have the advantage that they can be applied to a broad range of equations and many of them can be made to be high-order; a significant effort has been made toward the efficiency of these schemes. However, the fact that they involve discretizations of the differential operators can make them poorly conditioned. This is of particular concern when adaptive discretizations are required, such as when the surface, right hand side, or PDE coefficients have sharp features. Another class of methods that is commonly applied to solve surface PDEs are level set methods [7, 53, 54, 67]. These methods rely on formulas which relate finite differences in the volume around a surface to the intrinsic surface differentials themselves. Lastly, there exist a class of methods known as *closest point methods* [15, 46] which use an underlying representation of the surface in terms of *closest points*. The associated embedding is then discretized using finite differences, similar in style to when solving PDEs via level set methods. As both of these schemes also involve the discretized differential operators, they can suffer from the same conditioning problems as other direct methods.

For these reasons and others, we wish to consider methods that don't involve discretizing differential operators. In particular, we wish to convert the surface PDE into an integral equation. This has the advantage that when the integral equation is Fredholm second-kind, it is generally as well-conditioned as the underlying physical problem and can be solved accurately with high-order quadrature schemes that have been developed over the past several decades. Furthermore, discretized integral equations can often be solved asymptotically fast when combined with hierarchical compression methods, such as the fast multipole method (FMM) [36]. Integral equation methods have previously been used to solve the Laplace-Beltrami problem, but have required discretizing the composition of a large number of weakly singular operators [1, 62], or have only been applied to specific geometries, such as axisymmetric surfaces [26, 63] or spheres [2, 48, 49]. Other surface PDEs have not received as much attention and there only exist integral equation methods for constant coefficient PDEs on subsets of the sphere [49].

In this paper, we present a parametrix (also referred to as an approximate Green's function or Lévy function) for (1.1) and use it to convert (1.1) into an integral equation. As we shall see below, if the kernel of an integral operator is a parametrix for a PDE, then preconditioning the PDE with that operator results in a Fredholm second-kind integral equation. Parametrix based methods have been used to solve elliptic problems in the plane [8, 16–19, 31, 32], but have not been widely applied to problems along surfaces (despite the underlying theory being closely related). Our method can be thought of as an extension of the method presented in [48] to more general equations and surfaces. In [48], it was shown that the Green's function for the Poisson equation in the plane gives the Green's function for the Laplace-Beltrami problem on a sphere, up to an additive constant function. In this paper, we build on this observation and use the Green's functions for the Poisson and Helmholtz equations in the plane to find a parametrix for (1.1) on general smooth surfaces. We then use this parametrix to turn (1.1) into an integral equation and present a method for solving that integral equation numerically.

A parametrix-based integral equation has a few key advantages over other integral equation methods relying on Calderón-type identities or other potential-theoretic manipulations. First, the integral equation involves only a single integral operator with a kernel that is less singular than those required in the existing method for solving the Laplace-Beltrami problem on general surfaces [62]. Second, the approach is immediately applicable to a broad range of equations along any smooth surface. Finally, as demonstrated later on, using the parametrix as an analogue for the Green's

function allows for associated formulations for solving *surface boundary value problems*, i.e. elliptic surface PDE problems on surfaces with boundary and specified conditions along such boundaries.

The rest of the paper is divided into seven sections: in Section 2, we define a parametrix, recall some standard definitions for surface differential operators, and discuss existence and uniqueness properties of the Laplace-Beltrami problem. In Section 3, we introduce a parametrix and prove that it can be used to solve the Laplace-Beltrami problem. After discussing this simpler case, in Section 4 we discuss existence and uniqueness of solutions to (1.1); extensions of the parametrix to the more general case are addressed as well. Then, in Section 5, we discuss how our parametrix can be used to solve surface elliptic boundary value problems. In Section 6, we describe a method for discretizing the integral equations derived in the previous sections. In Section 7, we describe some numerical experiments that were used to verify the accuracy and efficiency of our method. Finally, in Section 8, we present some concluding remarks about this method and present some ways to extend this method to other problems.

2 Analytical preliminaries

In this section, we give the definition of a parametrix and discuss the motivation behind the definition and the typical uses of parametrices. Afterwards, we define the necessary surface differential operators and give the weak form of (1.1). Finally, we discuss the solvability of the Laplace-Beltrami problem. The solvability of other elliptic PDEs on surfaces is more complicated, and so is left to Section 4.

2.1 Parametrix basics

Let \mathcal{L} be a second order elliptic operator. A function $G(\mathbf{x}, \mathbf{x}')$ is said to be a Green's function for \mathcal{L} if

$$\mathcal{L}G(\mathbf{x}, \mathbf{x}') = \delta(\mathbf{x} - \mathbf{x}') \quad (2.1)$$

for each \mathbf{x}' in the domain in question. For most such \mathcal{L} , the exact Green's function G is not known in closed form; however, it is often possible to find a function $K = K(\mathbf{x}, \mathbf{x}')$ such that

$$\mathcal{L}K(\mathbf{x}, \mathbf{x}') = \delta(\mathbf{x} - \mathbf{x}') + R(\mathbf{x}, \mathbf{x}') \quad (2.2)$$

for all \mathbf{x}' . If R is reasonably well-behaved (as clarified below), then such a function K can be useful for both analytical and numerical work. We now define a particular class of K 's with a notion of well-behaved remainder functions R .

Definition 1 (Parametrix [16]). *Let \mathcal{L} be a second order differential operator. The function $K(\mathbf{x}, \mathbf{x}')$ is said to be a parametrix for \mathcal{L} if $\mathcal{L}K(\mathbf{x}, \mathbf{x}') = \delta(\mathbf{x} - \mathbf{x}') + R(\mathbf{x}, \mathbf{x}')$, where the remainder function R is an integrable function of \mathbf{x} e.g. the remainder function is $\mathcal{O}(\|\mathbf{x} - \mathbf{x}'\|^\alpha)$ with $\alpha > -2$ as $\mathbf{x} \rightarrow \mathbf{x}'$ on a two dimensional surface.*

Parametrices exist for other kinds of differential operators, with different conditions on the remainder function, but in this paper, we only consider second order elliptic problems and so the definition is sufficient. It is clear that a Green's function is a parametrix with remainder $R = 0$. For this reason, it is also common to refer to a parametrix as an approximate Green's function.

Historically, parametrices are used to prove existence for equations with non-analytic coefficients (see [34]), though they have also been used for computational methods. Much of this work uses the method for deriving parametrices that was introduced in [39] and is summarized in [42]. This classical parametrix is poorly suited for our purposes because it is written in terms of induced geodesic coordinates. We will therefore use a different parametrix, which will be much easier to evaluate numerically and give a remainder function that is smooth enough for our purposes.

2.2 Surface basics

In this section, we introduce some standard notation and ideas for working with differential equations defined on smooth surfaces. We define the standard differential operators and the weak form of (1.1). Throughout this section, we assume that the surface Γ is smooth and is given as the boundary of an open and bounded domain $\Omega \subset \mathbb{R}^3$. We shall discuss the standard differential operators on a surface through the use of a single (local) parameterization.

Definition 2. *Let Γ be a smooth surface and let $\mathbf{y} = \mathbf{y}(s, t)$ be a local parameterization with image $\Gamma_{\mathbf{y}}$. We can make the following definitions.*

1. *The surface metric associated with \mathbf{y} is*

$$g = \begin{bmatrix} \partial_s \mathbf{y} \cdot \partial_s \mathbf{y} & \partial_s \mathbf{y} \cdot \partial_t \mathbf{y} \\ \partial_s \mathbf{y} \cdot \partial_t \mathbf{y} & \partial_t \mathbf{y} \cdot \partial_t \mathbf{y} \end{bmatrix}. \quad (2.3)$$

2. *The surface gradient of a function f is*

$$\nabla_{\Gamma} f(\mathbf{x}) = [\mathbf{y}_s \quad \mathbf{y}_t] g^{-1} \begin{bmatrix} \partial_s \\ \partial_t \end{bmatrix} f. \quad (2.4)$$

3. *If a tangential vector field \mathbf{v} is written as $\mathbf{v}|_{\Gamma_{\mathbf{x}}} = v_s \mathbf{y}_s + v_t \mathbf{y}_t$, then the surface divergence is given by the formula*

$$\nabla_{\Gamma} \cdot \mathbf{v}(\mathbf{y}(s, t)) = \frac{1}{\sqrt{\det g}} \begin{bmatrix} \partial_s & \partial_t \end{bmatrix} \sqrt{\det g} \begin{bmatrix} v_s \\ v_t \end{bmatrix}. \quad (2.5)$$

The above definitions allow us to write and enforce (1.1) on the space of smooth functions. For this reason it is called a strong form PDE. In what follows, however, the weak form of (1.1) will allow us to use the tools of functional analysis to find conditions for existence of solutions to (1.1) and allow us to simplify subsequent proofs regarding a one-to-one correspondence of (1.1) and the associated integral equation. The weak form of a PDE is an equation over the Sobolev space

$$H^1(\Gamma) := \{ \rho \in L^2(\Gamma) : \nabla_{\Gamma} \rho \in (L^2(\Gamma))^3 \}, \quad (2.6)$$

which is a Hilbert space with inner product

$$(\sigma, \rho)_{H^1(\Gamma)} = \int_{\Gamma} (\bar{\rho} \sigma + \nabla_{\Gamma} \bar{\rho} \cdot \nabla_{\Gamma} \sigma). \quad (2.7)$$

With this space defined, we say that the weak form of (1.1) is

$$\int_{\Gamma} (-a \nabla_{\Gamma} \bar{\rho} \cdot \nabla_{\Gamma} u + \bar{\rho} \mathbf{b} \cdot \nabla_{\Gamma} u + c \bar{\rho} u) = \int_{\Gamma} \bar{\rho} f, \quad \text{for all } \rho \in H^1(\Gamma). \quad (2.8)$$

A function $u \in H^1(\Gamma)$ that solves (2.8) is called a weak solution of (1.1). A simple integration-by-parts argument gives that a function $u \in C^2(\Gamma)$ is a solution of (1.1) if and only if it is a weak solution (see [45]).

We end this section with two more definitions: We shall let \mathbf{n} be the outward unit normal to Γ and $H = \frac{1}{2} \nabla_{\Gamma} \cdot \mathbf{n}$ be the mean curvature of Γ .

2.3 Existence and uniqueness for the Laplace-Beltrami problem

In this section, we will see that the Laplace-Beltrami problem is well-posed when its domain and range are chosen correctly.

By inspection, the Laplace-Beltrami operator (1.2) annihilates constants. For this reason, the solution of the Laplace-Beltrami problem on a closed surface can only be determined up to an additive constant. In order for the equation to have a unique solution, we will therefore assume

that the solution u has zero mean. It is also necessary to restrict the range of the Laplace-Beltrami problem: if we plug a constant ρ into the weak form (2.8), then (2.8) is unsolvable if f has a non-zero mean. When we combine these observations, it becomes clear that we should view the Laplace-Beltrami operator as a map from mean-zero functions to themselves.

In order to include these restrictions in the weak form of (1.2), we define the function space

$$H_{\text{mz}}^1(\Gamma) := \left\{ \rho \in H^1(\Gamma) : \int_{\Gamma} \rho = 0 \right\}, \quad (2.9)$$

which is also a Hilbert space with inner product $(\cdot, \cdot)_{H^1(\Gamma)}$. Since we need it below, we also define $L_{\text{mz}}^2(\Gamma)$ as the subset of $L^2(\Gamma)$ with mean zero.

With these function spaces, the weak form of (1.2) becomes

$$-\int_{\Gamma} \nabla_{\Gamma} u \cdot \nabla_{\Gamma} \rho = \int_{\Gamma} f \rho, \quad \text{for all } \rho \in H_{\text{mz}}^1(\Gamma), \quad (2.10)$$

where $f \in L_{\text{mz}}^2(\Gamma)$. As before, a smooth function u is a solution of (1.1) if and only if it is a solution of (2.10). The following theorem gives that this weak form is well posed.

Theorem 1. *If Γ is a smooth and closed surface, then for every mean-zero right hand side $f \in L_{\text{mz}}^2(\Gamma)$ there exists a unique mean-zero solution $u \in H_{\text{mz}}^1(\Gamma)$ of (1.2).*

This theorem is an immediate consequence of a subsequent result in the manuscript, Theorem 7, with $a = 1$ and $c = 0$. It is also well-known on its own. Theorem 1 can be extended to give higher regularity on the solution u . In [73], it is shown that if the right hand side is in a higher order Sobolev space, then it is possible to control the norm of the higher order derivatives of u , but we omit such discussions from this work for the sake of brevity.

3 A parametrix for the Laplace-Beltrami problem

In this section, we introduce a parametrix for the Laplace-Beltrami problem (1.2) on a smooth and closed surface Γ . We then use that parametrix to convert (1.2) into an equivalent integral equation. We save the discussion of general elliptic equations for Section 4.2.

The function

$$G(r) = \frac{1}{2\pi} \log r$$

is the free-space Green's function for the Laplace operator in \mathbb{R}^2 . An analogous function can be defined in \mathbb{R}^3 , as in [48]:

$$K_{\text{LB}}(\mathbf{x}, \mathbf{x}') = \frac{1}{2\pi} \log \|\mathbf{x} - \mathbf{x}'\| \quad (3.1)$$

for all $\mathbf{x}, \mathbf{x}' \in \mathbb{R}^3$ with $\mathbf{x} \neq \mathbf{x}'$. The smoothness of Γ will give that K_{LB} is a parametrix for the Laplace-Beltrami problem.

Theorem 2. *If Γ is a smooth closed surface, then K_{LB} is a candidate parametrix for the Laplace-Beltrami equation, i.e.*

$$\Delta_{\Gamma} K_{\text{LB}}(\mathbf{x}, \mathbf{x}') = \delta(\mathbf{x} - \mathbf{x}') + R_{\text{LB}}(\mathbf{x}, \mathbf{x}'), \quad (3.2)$$

where the derivatives in Δ_{Γ} are taken with respect to \mathbf{x} . Furthermore, for $\mathbf{x} \neq \mathbf{x}'$, the remainder function is

$$R_{\text{LB}}(\mathbf{x}, \mathbf{x}') = \frac{1}{\pi} \left(\frac{\mathbf{n}(\mathbf{x}) \cdot \mathbf{r}}{r^2} \right)^2 - \frac{H(\mathbf{x})}{\pi} \frac{\mathbf{n}(\mathbf{x}) \cdot \mathbf{r}}{r^2}, \quad (3.3)$$

where $\mathbf{r} = \mathbf{x} - \mathbf{x}'$ and $r = \|\mathbf{r}\|$.

Proof. We begin by choosing a parameterization such that $\mathbf{x}' = \mathbf{y}(\mathbf{0})$, and define $C_R(\mathbf{x}') := \mathbf{y}(C_R(\mathbf{0}))$ and $B_R(\mathbf{x}') := \mathbf{y}(B_R(\mathbf{0}))$ to be the image of the circle and ball of radius R centered at \mathbf{x}' , respectively. Since K_{LB} is smooth for $\mathbf{x} \neq \mathbf{x}'$, showing (3.2) is equivalent to showing that

$$\lim_{R \rightarrow 0} \int_{B_R(\mathbf{x}')} \Delta_{\Gamma} K_{\text{LB}}(\cdot, \mathbf{x}') \varphi = \varphi(\mathbf{x}'), \quad (3.4)$$

for all smooth test functions φ , where the Laplace-Beltrami operator is interpreted in a weak sense.

First, by the definition of the weak derivative, we have that

$$\int_{\Gamma} \Delta_{\Gamma} K_{\text{LB}}(\cdot, \mathbf{x}') \varphi = \int_{\Gamma} K_{\text{LB}}(\cdot, \mathbf{x}') \Delta_{\Gamma} \varphi. \quad (3.5)$$

Next, for $R > 0$, manipulating the domains of integration, using (3.5), and applying Green's third identity gives that

$$\begin{aligned} \int_{B_R(\mathbf{x}')} \Delta_{\Gamma} K_{\text{LB}}(\cdot, \mathbf{x}') \varphi &= \int_{\Gamma} K_{\text{LB}}(\cdot, \mathbf{x}') \Delta_{\Gamma} \varphi - \int_{\Gamma \setminus B_R(\mathbf{x}')} \Delta_{\Gamma} K_{\text{LB}}(\cdot, \mathbf{x}') \varphi \\ &= \int_{B_R(\mathbf{x}')} K_{\text{LB}}(\cdot, \mathbf{x}') \Delta_{\Gamma} \varphi + \int_{C_R(\mathbf{x}')} \boldsymbol{\nu} \cdot \nabla_{\Gamma} K_{\text{LB}}(\cdot, \mathbf{x}') \varphi \\ &\quad - \int_{C_R(\mathbf{x}')} K_{\text{LB}}(\cdot, \mathbf{x}') \boldsymbol{\nu} \cdot \nabla_{\Gamma} \varphi, \end{aligned} \quad (3.6)$$

where $\boldsymbol{\nu}$ is the unit *binormal* vector to $C_R(\mathbf{x}')$, which is defined to be tangent to Γ , normal $C_R(\mathbf{x}')$, and to point away from $B_R(\mathbf{x}')$. The first and third terms above will vanish as $R \rightarrow 0$ due to the smoothness of φ and the weak logarithmic singularity in K_{LB} . For the second term, we add and subtract $\varphi(\mathbf{x}')$, yielding:

$$\begin{aligned} \int_{C_R(\mathbf{x}')} \boldsymbol{\nu} \cdot \nabla_{\Gamma} K_{\text{LB}}(\cdot, \mathbf{x}') \varphi &= \int_{C_R(\mathbf{x}')} \boldsymbol{\nu} \cdot \nabla_{\Gamma} K_{\text{LB}}(\cdot, \mathbf{x}') \varphi \\ &\quad + \int_{C_R(\mathbf{x}')} \boldsymbol{\nu} \cdot \nabla_{\Gamma} K_{\text{LB}}(\cdot, \mathbf{x}') (\varphi - \varphi(\mathbf{x}')). \end{aligned} \quad (3.7)$$

Since φ is smooth, and K_{LB} has a logarithmic singularity, the second term vanishes as $R \rightarrow 0$. We therefore have that

$$\lim_{R \rightarrow 0} \int_{\Gamma \cap B_R(\mathbf{x}')} \Delta_{\Gamma} K_{\text{LB}}(\cdot, \mathbf{x}') \varphi = \varphi(\mathbf{x}') \lim_{R \rightarrow 0} \int_{\Gamma \setminus B_R(\mathbf{x}')} \boldsymbol{\nu} \cdot \nabla_{\Gamma} K_{\text{LB}}(\cdot, \mathbf{x}'). \quad (3.8)$$

We now show that the right hand limit is equal to one. First, we note that

$$\boldsymbol{\nu} = \frac{\mathbf{x} - \mathbf{x}'}{\|\mathbf{x} - \mathbf{x}'\|} + \mathcal{O}(R)$$

and define I_R by

$$\begin{aligned} I_R &:= \int_{C_R(\mathbf{x}')} \boldsymbol{\nu} \cdot \nabla_{\Gamma} K_{\text{LB}}(\cdot, \mathbf{x}') \\ &= \int_{C_R(\mathbf{x}')} \left(\frac{\mathbf{x} - \mathbf{x}'}{\|\mathbf{x} - \mathbf{x}'\|} + \mathcal{O}(R) \right) \cdot \frac{\mathbf{x} \cdot \nabla_{\Gamma} \mathbf{x}}{2\pi \|\mathbf{x} - \mathbf{x}'\|^2}. \end{aligned} \quad (3.9)$$

We next parameterize $C_R(\mathbf{x}')$ by $\mathbf{y}(\Phi_R(\theta))$ where $\Phi_R(\theta) := R [\cos \theta \quad \sin \theta]^T$. Taylor expanding \mathbf{y} around the origin gives that

$$I_R = \int_0^{2\pi} \left(\frac{g(\mathbf{0}) \Phi_R(\theta)}{R} + \mathcal{O}(R) \right)^T \frac{g^{-1}(\mathbf{0}) \Phi_R(\theta) + \mathcal{O}(R^2)}{2\pi R^2 + \mathcal{O}(R^3)} R d\theta + \mathcal{O}(R). \quad (3.10)$$

Some more simplification gives

$$I_R = (2\pi)^{-1} \int_0^{2\pi} R^{-2} \Phi_R(\theta)^T g(\mathbf{0}) g^{-1}(\mathbf{0}) \Phi_R(\theta) d\theta + \mathcal{O}(R). \quad (3.11)$$

Evaluating this integral gives

$$I_R = 1 + \mathcal{O}(R), \quad (3.12)$$

which, when combined with (3.8), proves (3.4) and so that K_{LB} is a candidate to be a parametrix.

The expression for the remainder (3.3) is obtained from the following formula for the surface Laplacian of a smooth function defined in a neighborhood of Γ (see [60]), which will be valid wherever K_{LB} is smooth, i.e. for $\mathbf{x} \neq \mathbf{x}'$:

$$\begin{aligned} R_{LB}(\mathbf{x}, \mathbf{x}') &= \Delta_\Gamma K_{LB}(\mathbf{x}, \mathbf{x}') \\ &= \Delta K_{LB}(\mathbf{x}, \mathbf{x}') - \partial_{\mathbf{n}(\mathbf{x})}^2 K_{LB}(\mathbf{x}, \mathbf{x}') - 2H(\mathbf{x}) \partial_{\mathbf{n}(\mathbf{x})} K_{LB}(\mathbf{x}, \mathbf{x}'). \end{aligned} \quad (3.13)$$

□

We now verify that K_{LB} is indeed a parametrix for the Laplace-Beltrami problem by showing that R_{LB} is integrable.

Theorem 3. *If Γ is a smooth surface, then $R_{LB}(\mathbf{x}, \mathbf{x}') = \mathcal{O}(1)$ as $\mathbf{x}' \rightarrow \mathbf{x}$ and K_{LB} is a parametrix for the Laplace-Beltrami problem.*

Proof. By Theorem 2, it is enough to show the first statement.

Let γ be a curve along Γ , passing through \mathbf{x} , obtained from the intersection of a plane normal to Γ at \mathbf{x} with Γ . We shall show that $R_{LB}(\mathbf{x}, \gamma(s))$ is a continuous function of s , where $\gamma(s)$ is an arclength parameterization of γ .

We suppose that $\gamma(\tilde{s}) = \mathbf{x}$. As an intermediate step, we Taylor expand γ and compute

$$\lim_{s \rightarrow \tilde{s}} \frac{\mathbf{n}(\mathbf{x}) \cdot (\gamma(\tilde{s}) - \gamma(s))}{\|\gamma(\tilde{s}) - \gamma(s)\|^2} = \lim_{s \rightarrow \tilde{s}} \frac{\mathbf{n}(\mathbf{x}) \cdot \left((\tilde{s} - s)\gamma'(\tilde{s}) + \frac{(\tilde{s} - s)^2}{2}\gamma''(\tilde{s}) + \mathcal{O}((\tilde{s} - s)^3) \right)}{(\tilde{s} - s)^2 \|\gamma'(s)\|^2 + \mathcal{O}((\tilde{s} - s)^4)}. \quad (3.14)$$

Since γ is parameterized by arclength, $\|\gamma'\| = 1$, $\mathbf{n}(\mathbf{x}) \cdot \gamma'(\tilde{s}) = 0$, and $\mathbf{n}(\mathbf{x}) \cdot \gamma''(\tilde{s}) = \kappa_\gamma$, where κ_γ is the curvature of γ at \mathbf{x} . The limit thus becomes

$$\lim_{s \rightarrow \tilde{s}} \frac{\mathbf{n}(\mathbf{x}) \cdot (\gamma(\tilde{s}) - \gamma(s))}{\|\gamma(\tilde{s}) - \gamma(s)\|^2} = \frac{\kappa_\gamma}{2}. \quad (3.15)$$

Inserting this limit into (3.3), we obtain

$$\begin{aligned} \lim_{s \rightarrow \tilde{s}} R_{LB}(\gamma(\tilde{s}), \gamma(s)) &= \lim_{s \rightarrow \tilde{s}} \left[2 \left(\frac{\mathbf{n}(\mathbf{x}) \cdot (\gamma(\tilde{s}) - \gamma(s))}{\|\gamma(\tilde{s}) - \gamma(s)\|^2} \right)^2 - 2H(\mathbf{x}) \frac{\mathbf{n}(\mathbf{x}) \cdot (\gamma(\tilde{s}) - \gamma(s))}{\|\gamma(\tilde{s}) - \gamma(s)\|^2} \right] \\ &= \frac{\kappa_\gamma^2}{2} - H(\mathbf{x})\kappa_\gamma. \end{aligned} \quad (3.16)$$

The curvature κ_γ will vary between the principal curvatures κ_1 and κ_2 , depending on the angle of approach. Specifically, if θ is the angle between the first principal direction and $\gamma'(\tilde{s})$, then

$$\kappa_\gamma(\theta) = \kappa_1 \cos^2(\theta) + \kappa_2 \sin^2(\theta). \quad (3.17)$$

Using this expression for the curvature and writing the principal curvatures in terms of the mean and Gaussian curvatures gives that

$$\lim_{s \rightarrow \tilde{s}} R_{LB}(\gamma(\tilde{s}), \gamma(s)) = -\frac{H^2(\mathbf{x}) \sin^2(2\theta) + \kappa_G(\mathbf{x}) \cos^2(2\theta)}{4\pi}, \quad (3.18)$$

where $\kappa_G(\mathbf{x})$ is the Gaussian curvature of the surface at \mathbf{x} . Since the surface is smooth, this limit is bounded, and therefore $R_{LB}(\mathbf{x}, \mathbf{x}')$ is $\mathcal{O}(1)$ as $\mathbf{x}' \rightarrow \mathbf{x}$. □

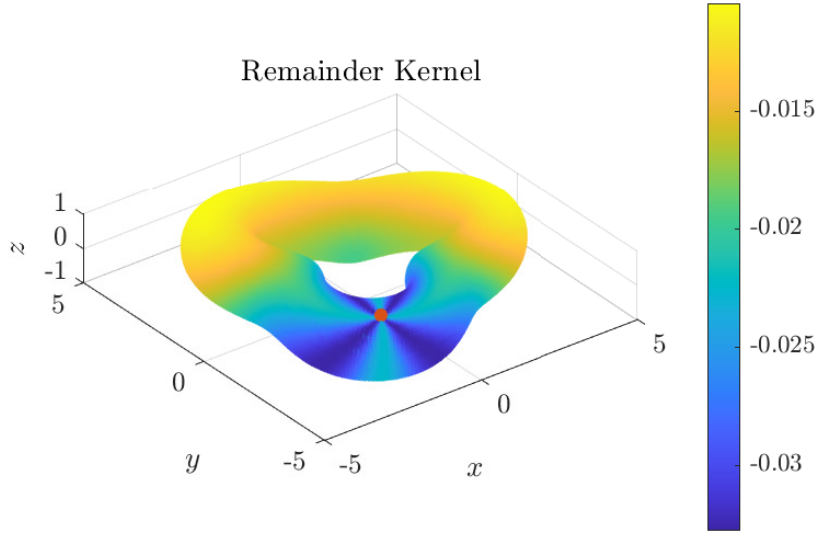


Figure 1: This plot shows the remainder kernel $R_{LB}(\mathbf{x}, \cdot)$ for the Laplace-Beltrami problem on an example surface. We see that it is bounded, but not smooth around \mathbf{x} (red dot).

We shall pause here to note that the above proof gives that the remainder function is not smooth as $\mathbf{x}' \rightarrow \mathbf{x}$ because $R_{LB}(\mathbf{x}, \mathbf{x}')$ depends on the direction of approach. A plot of the remainder kernel along a toroidal like object, for a fixed \mathbf{x} , is shown in Figure 1.

We can now show that using this parametrix yields a second-kind integral equation for the Laplace-Beltrami problem along general smooth surfaces.

Theorem 4. *The integral equation*

$$\sigma(\mathbf{x}) + \int_{\Gamma} R_{LB}(\mathbf{x}, \mathbf{x}') \sigma(\mathbf{x}') da(\mathbf{x}') = f(\mathbf{x}), \quad \mathbf{x} \in \Gamma, \quad (3.19)$$

is a second-kind Fredholm integral equation on $L^2(\Gamma)$. Furthermore, if $f \in L^2_{mz}(\Gamma)$ and σ is the solution of (3.19), then the function

$$\begin{aligned} u(\mathbf{x}) &= \mathcal{K}_{LB}[\sigma](\mathbf{x}) \\ &= \int_{\Gamma} K_{LB}(\mathbf{x}, \mathbf{x}') \sigma(\mathbf{x}') da(\mathbf{x}') \end{aligned} \quad (3.20)$$

is the unique mean-zero solution of the Laplace-Beltrami problem.

Proof. We begin by noting that the remainder function is bounded. The integral operator

$$\mathcal{R}_{LB}[\sigma](\mathbf{x}) = \int_{\Gamma} R_{LB}(\mathbf{x}, \mathbf{x}') \sigma(\mathbf{x}') da(\mathbf{x}') \quad (3.21)$$

is therefore a Hilbert-Schmidt operator and so is compact as a map from $L^2(\Gamma)$ to itself by Theorem 0.45 in [29]. The equation (3.19) is therefore a second-kind Fredholm integral equation.

We shall now verify that when σ solves (3.19), the formula in (3.20) gives a weak solution of (1.2), i.e., that for all $\varphi \in C^2(\Gamma)$

$$- \int_{\Gamma} \nabla_{\Gamma} u \cdot \nabla_{\Gamma} \varphi = \int_{\Gamma} f \varphi. \quad (3.22)$$

Integrating by parts in the above expression and plugging in the representation for u gives us that

$$\int_{\Gamma} u \Delta_{\Gamma} \varphi = \int_{\Gamma} \left(\int_{\Gamma} K_{\text{LB}}(\mathbf{x}, \mathbf{x}') \sigma(\mathbf{x}') da(\mathbf{x}') \right) \Delta_{\Gamma} \varphi(\mathbf{x}) da(\mathbf{x}). \quad (3.23)$$

We note that since (3.19) is Fredholm second-kind, σ will be in $L^2_{\text{mz}}(\Gamma)$. Since K_{LB} is also integrable, we may use Fubini's theorem to find that

$$\int_{\Gamma} u \Delta_{\Gamma} \varphi = \int_{\Gamma} \sigma(\mathbf{x}') \int_{\Gamma} K_{\text{LB}}(\mathbf{x}, \mathbf{x}') \Delta_{\Gamma} \varphi(\mathbf{x}) da(\mathbf{x}) da(\mathbf{x}'). \quad (3.24)$$

We now wish to bring the derivatives on φ onto K_{LB} . We do this by integrating by parts in the weak sense. Since we have computed the weak derivative of K_{LB} in Theorem 2, we have that

$$\begin{aligned} \int_{\Gamma} u \Delta_{\Gamma} \varphi &= \int_{\Gamma} \sigma(\mathbf{x}') \int_{\Gamma} \Delta_{\Gamma} K_{\text{LB}}(\mathbf{x}, \mathbf{x}') \varphi(\mathbf{x}) da(\mathbf{x}) da(\mathbf{x}') \\ &= \int_{\Gamma} \sigma(\mathbf{x}') \left(\varphi(\mathbf{x}') + \int_{\Gamma} R_{\text{LB}}(\mathbf{x}, \mathbf{x}') \varphi(\mathbf{x}) da(\mathbf{x}) \right) da(\mathbf{x}'). \end{aligned} \quad (3.25)$$

Another application of Fubini's theorem combined with a change of variables gives

$$\begin{aligned} \int_{\Gamma} u \Delta_{\Gamma} \varphi &= \int_{\Gamma} \varphi(\mathbf{x}) \left(\sigma(\mathbf{x}) + \int_{\Gamma} R_{\text{LB}}(\mathbf{x}, \mathbf{x}') \sigma(\mathbf{x}') da(\mathbf{x}') \right) da(\mathbf{x}) \\ &= \int_{\Gamma} \varphi f. \end{aligned} \quad (3.26)$$

Thus $\Delta_{\Gamma} u = f$ in the weak sense, and so u is the desired solution. \square

The integral equation in (3.19) involves the operator $\mathcal{I} + \mathcal{R}_{\text{LB}}$, which is the composition of the Laplace-Beltrami operator with \mathcal{K}_{LB} . It is therefore *not* solvable for any right hand side with non-zero mean. Since (3.19) is Fredholm second-kind, it must therefore have at least a one-dimensional null-space consisting of functions that are mapped to constants by \mathcal{K}_{LB} . For numerical reasons, it is often advantageous to modify this equation so that it is uniquely invertible for *any* right-hand side, and handle the mean-zero constraint separately and explicitly. We can do this by adding the term $\int_{\Gamma} \sigma$.

This kind of one-dimensional update is discussed in detail [65]. In short, this update makes the solution of (3.19) unique by fixing the projection of the solution onto the null vector, which we denote by σ_n . This method is known to remove the null-space of the integral equation provided that σ_n has a non-zero mean. While there is no formula for σ_n on general surfaces, some calculus shows that if Γ is a sphere, then σ_n is a constant function and if Γ is a torus, then $\sigma_n = \alpha - \rho$, where $\rho = \rho(\mathbf{x})$ is the distance from \mathbf{x} to the axis of rotation. The constant α depends on the inner and outer radii of the torus, but is not the mean of $\sqrt{x^2 + y^2}$ over Γ .

We now make the following conjecture:

Conjecture 1. *The integral equation (3.19) has only a one-dimensional null space on all smooth surfaces.*

This conjecture is based on a few observations:

1. When Γ is a sphere, the work in [48] showed that $R_{\text{LB}} = 1/|\Gamma|$. The integral equation (3.19) thus becomes $\sigma - \hat{\sigma} = f$, where $\hat{\sigma}$ is the mean of σ , which clearly has only a one-dimensional null space for any sized sphere.
2. The associated discretization of the integral equation had only one zero singular value for all of the surfaces considered in subsequent numerical examples (Section 7), which include examples of genus 0 and genus 1.

3. The integral equation (3.19) is invariant under surface dilation. By this we mean that if $a\Gamma = \{a\mathbf{x} \text{ such that } \mathbf{x} \in \Gamma\}$, then $\mathcal{R}_{\text{LB},a\Gamma}[\sigma](a\mathbf{x}) = \mathcal{R}_{\text{LB},\Gamma}[\sigma](\mathbf{x})$ for all $a > 0$. This implies that the sign change in the parametrix at $\|\mathbf{x} - \mathbf{x}'\| = 1$ does not introduce a null space, since Γ can be assumed to have a diameter less than 1.

In addition to being interesting in and of itself, proving the above conjecture would have computational ramifications, as the discretized linear systems could be solved by any preferred means (iteratively, directly, etc.) without worry of unknown rank deficiencies.

4 Elliptic PDEs on surfaces

The above parametrix method may be extended to a broader class of surface elliptic equations of the form (1.1). In this section, we introduce this class of equations and discuss solvability conditions and introduce our parametrix. For simplicity, we shall assume that $\mathbf{b} = 0$. Introducing a non-zero \mathbf{b} only requires minor changes, and is discussed in Section 4.3.

4.1 Existence of solutions

In this section, we shall discuss some aspects of existence and uniqueness of (1.1); a thorough investigation of conditions under which (1.1) is well-posed is beyond the scope of this paper. Instead, we present Theorems 7, 9, and 10 as examples of such conditions, and the results which they lead to.

In order to prove these theorems, we shall need following two well-known theorems.

Theorem 5 (Poincaré's inequality for surfaces (Theorem 2.10 in [40])). *If Γ is a smooth surface then there exists a constant $C_\Gamma > 0$ such that for every function $u \in H^1(\Gamma)$,*

$$\int_\Gamma |u - \hat{u}|^2 \leq C_\Gamma \int_\Gamma \|\nabla_\Gamma u\|^2, \quad (4.1)$$

where \hat{u} is the mean of u .

Theorem 6 (Lax-Milgram (see [12])). *Let \mathcal{H} be a Hilbert space and the sesquilinear form $\mathcal{B}(u, \rho)$ be bounded and coercive on \mathcal{H} , i.e.*

$$|\mathcal{B}(u, \rho)| \leq C_B \|u\|_{\mathcal{H}} \|\rho\|_{\mathcal{H}} \quad \text{and} \quad \Re(\xi \mathcal{B}(u, u)) \geq C_C \|u\|_{\mathcal{H}}^2, \quad (4.2)$$

for some positive constants C_B, C_C , and some $\xi \in \mathbb{C}$ with $|\xi| = 1$. *If the conjugate linear form $\mathcal{A}(\rho)$ is bounded, i.e.*

$$|\mathcal{A}(\rho)| \leq C_A \|\rho\|_{\mathcal{H}} \quad (4.3)$$

for some positive constant C_A , then there exists a unique $u \in \mathcal{H}$ such that $\mathcal{B}(u, \rho) = \mathcal{A}(\rho)$ for all $\rho \in \mathcal{H}$.

We are now ready to prove an existence theorem for (1.1) given some mildly restrictive conditions on a and c . The proof of the first statement appeared in [23], and the proof of the second is very similar to the equivalent problem in subsets of \mathbb{R}^n considered in example 9.5.3 in [12].

Theorem 7. *Let Γ be a smooth and closed surface and f be in $L^2(\Gamma)$. If one of the following holds, then there exists a weak solution $u \in H^1(\Gamma)$ of (1.1):*

1. *The coefficient function c is identically zero and f is mean-zero.*
2. *There exists a $\theta \in (-\frac{\pi}{2}, \frac{\pi}{2})$ such that $\Re(ce^{i\theta}) < 0$.*

Furthermore, the solution is unique if condition 2 holds. If condition 1 holds, then there is a unique mean-zero solution.

Proof. We begin by defining the sesquilinear form

$$\mathcal{B}(u, \rho) = \int_{\Gamma} (-a \nabla_{\Gamma} \bar{\rho} \cdot \nabla_{\Gamma} u + c \bar{\rho} u) \quad (4.4)$$

and the conjugate linear form

$$\mathcal{A}(\rho) = \int_{\Gamma} f \bar{\rho}. \quad (4.5)$$

With these definitions, the weak form (2.8) becomes the equation

$$\mathcal{B}(u, \rho) = \mathcal{A}(\rho), \quad \text{for all } \rho \in H^1(\Gamma). \quad (4.6)$$

We note that \mathcal{B} is bounded on $H^1(\Gamma) \times H^1(\Gamma)$:

$$\begin{aligned} |\mathcal{B}(u, \rho)| &\leq \max_{\Gamma} a \int_{\Gamma} |\nabla_{\Gamma} \bar{\rho} \cdot \nabla_{\Gamma} u| + \max_{\Gamma} |c| \int_{\Gamma} |\rho u| \\ &\leq \left(\max_{\Gamma} a + \max_{\Gamma} |c| \right) \|\rho\|_{H^1(\Gamma)} \|u\|_{H^1(\Gamma)}. \end{aligned} \quad (4.7)$$

The conjugate linear form \mathcal{A} is bounded on $H^1(\Gamma)$ via the Cauchy-Schwartz inequality.

We first consider Condition 1. In this case, constant functions are in the null space of the PDE and the range is mean-zero functions, as in the case of the Laplace-Beltrami problem. We shall therefore apply the Lax-Milgram theorem on the space $H_{mz}^1(\Gamma)$. The forms $\mathcal{B}(u, \rho)$ and $\mathcal{A}(\rho)$ are bounded on $H_{mz}^1(\Gamma)$ for the same reason that they are bounded on $H^1(\Gamma)$. To see that the sesquilinear form is coercive, we compute

$$-\mathcal{B}(u, u) = \int_{\Gamma} a \|\nabla_{\Gamma} u\|^2 \geq \min_{\Gamma} a \int_{\Gamma} \|\nabla_{\Gamma} u\|^2. \quad (4.8)$$

Applying the Poincaré inequality then gives that

$$\begin{aligned} -\mathcal{B}(u, u) &\geq \frac{\min_{\Gamma} a}{1 + C_{\Gamma}} \|\nabla_{\Gamma} u\|_{L^2(\Gamma)}^2 + \frac{\min_{\Gamma} a}{1 + C_{\Gamma}} \|u\|_{L^2(\Gamma)}^2 \\ &\geq \frac{\min_{\Gamma} a}{1 + C_{\Gamma}} \|u\|_{H^1(\Gamma)}^2. \end{aligned} \quad (4.9)$$

Since the multiplicative constant on the right hand side is positive, \mathcal{B} is coercive. The Lax-Milgram theorem then gives that there exists a unique $u \in H_{mz}^1(\Gamma)$ that solves (2.8).

We now consider Condition 2. Multiplying $\mathcal{B}(u, u)$ by $e^{i\theta}$ and taking the real part gives that

$$\begin{aligned} \Re(-e^{i\theta} \mathcal{B}(u, u)) &= \int_{\Gamma} \left(a \cos \theta \|\nabla_{\Gamma} u\|^2 - \Re(ce^{i\theta}) |u|^2 \right) \\ &\geq \cos \theta \min_{\Gamma} a \|\nabla_{\Gamma} u\|_{L^2(\Gamma)}^2 - \max_{\Gamma} \Re(ce^{i\theta}) \|u\|_{L^2(\Gamma)}^2. \end{aligned} \quad (4.10)$$

Since a is strictly positive, $\theta \in (-\frac{\pi}{2}, \frac{\pi}{2})$, and the real part of $ce^{i\theta}$ is strictly negative, we have that \mathcal{B} is coercive with constant

$$C_C = \min\{\cos \theta \min_{\Gamma} a, -\max_{\Gamma} \Re(ce^{i\theta})\} < 0.$$

The Lax-Milgram Theorem then gives that there exists a unique $u \in H^1(\Gamma)$ that solves (2.8). \square

Theorem 8. *Suppose that Γ is a smooth surface and the coefficient functions are smooth. If the solution u of (1.1) exists and the right hand side f is smooth, then u is also smooth.*

Proof. We prove this by mapping (1.1) to an elliptic equation in \mathbb{R}^2 and using standard regularity results. If $\mathbf{y} : U \rightarrow \Gamma$ is local parameterization of part of Γ , then the pull-back of the differential operator onto U is

$$\mathcal{E}v := (\nabla_{\Gamma} \cdot (a \nabla_{\Gamma} (v \circ \mathbf{y}))) \circ \mathbf{y}^{-1} + (c \circ \mathbf{y}^{-1})v. \quad (4.11)$$

Because \mathbf{y} is smooth, \mathcal{E} is an elliptic operator with smooth coefficients. Since we also have that $\mathcal{E}(u \circ \mathbf{y}) = f \circ \mathbf{y}$, Theorem 3 in Section 6.3.1 of [28] gives that $u \circ \mathbf{y}$ is smooth in the interior of the domain U . We therefore have that u is smooth on the interior of the range of \mathbf{y} . By choosing different parameterizations we can cover Γ and prove that u is smooth everywhere. \square

Helmholtz-type equations

As a special case, we now address existence and uniqueness for (1.1) when c is real and positive, which corresponds to equations of Helmholtz-type. This case is more complicated as the associated sesquilinear form will not be coercive. For simplicity, we suppose that $c > 0$ is constant and not zero. In this case, we can use an argument very similar to that used for the equivalent problem in the plane, see [28]. When c is constant, equation (1.1) is well-posed if and only if $-c$ is in the resolvent set of

$$\mathcal{L} := \nabla_{\Gamma} \cdot a \nabla_{\Gamma}. \quad (4.12)$$

We will study the resolvent set of \mathcal{L} by proving that its inverse, $\mathcal{S} := \mathcal{L}^{-1}$, is a self-adjoint and negative semi-definite compact operator. This will allow us to use the spectral theorem for compact operators, Theorem 28.3 in [51], to characterize the resolvent set of \mathcal{L} . We now formalize this argument.

Theorem 9 (Analogue of Theorem 6.2.5 in [28]). *Let \mathcal{S} be the map from functions $g \in L^2_{\text{mz}}(\Gamma)$ to the mean-zero solution v of $\mathcal{L}v = g$. If c is a non-zero constant function, then there exists a unique weak solution $u \in H^1(\Gamma)$ of (1.1) if and only if $-1/c$ is not in the spectrum of \mathcal{S} .*

Proof. Suppose that u and $f \in L^2_{\text{mz}}(\Gamma)$. If we apply \mathcal{S} to both sides of (1.1) and divide by c , we find that (1.1) becomes

$$\frac{1}{c}u + \mathcal{S}u = \frac{1}{c}\mathcal{S}f. \quad (4.13)$$

Since c was assumed to be constant, (4.13) (and thus (1.1)) is well-posed in $L^2_{\text{mz}}(\Gamma)$ if and only if $-1/c$ is not in the spectrum of \mathcal{S} .

We now suppose that $f \in L^2(\Gamma)$. In this case, we write $f = \tilde{f} + \hat{f}$, where \hat{f} is the mean of f , and write the function $u = \tilde{u} + \hat{u}$, where \hat{u} is the mean of u . Since c is constant, (1.1) is equivalent to the uncoupled equations

$$\begin{aligned} \nabla_{\Gamma} \cdot a \nabla_{\Gamma} \tilde{u} + c\tilde{u} &= \tilde{f}, \\ c\hat{u} &= \hat{f}. \end{aligned} \quad (4.14)$$

Since c is non-zero, there always exists a unique \hat{u} solving the second equation. The first equation is equivalent to the mean-zero case, and so has a unique solution if and only if $-1/c$ is not in the spectrum of \mathcal{S} , and we have the desired result. \square

We now verify the spectrum of \mathcal{S} is countable.

Theorem 10 (Analogue of Theorems 6.2.4 and 6.2.5 in [28]). *Let Γ be a smooth and closed surface and the function a be continuous and positive. The solution operator \mathcal{S} is a compact map from $L^2_{\text{mz}}(\Gamma)$ to itself. Furthermore, the spectrum of \mathcal{S} is real, positive, and countable.*

Proof. We suppose that $f, g \in L^2_{\text{mz}}(\Gamma)$ and that $v = \mathcal{S}g$. We also let

$$B(\mu, \rho) = - \int_{\Gamma} a \nabla_{\Gamma} \mu \cdot \nabla_{\Gamma} \bar{\rho}. \quad (4.15)$$

We begin by proving that \mathcal{S} is a bounded map from $L^2_{\text{mz}}(\Gamma)$ to $H^1_{\text{mz}}(\Gamma)$. By the definition of \mathcal{S} ,

$$B(v, v) = (g, v)_{L^2}. \quad (4.16)$$

The coerciveness of B discussed in the proof of Theorem 7 and the Cauchy-Schwartz inequality then give that

$$\begin{aligned} c\|v\|_{H^1(\Gamma)}^2 &\leq B(v, v) \\ &= (g, v)_{L^2} \\ &\leq \|g\|_{L^2(\Gamma)} \|v\|_{L^2(\Gamma)} \\ &\leq \|g\|_{L^2(\Gamma)} \|v\|_{H^1(\Gamma)} \end{aligned} \quad (4.17)$$

The operator \mathcal{S} is thus a bounded map from $L^2_{\text{mz}}(\Gamma)$ to $H^1_{\text{mz}}(\Gamma)$. Since $H^1_{\text{mz}}(\Gamma)$ is compactly embedded in $L^2_{\text{mz}}(\Gamma)$, we have that \mathcal{S} is a bounded and compact map from $L^2_{\text{mz}}(\Gamma)$ to itself.

We now prove that \mathcal{S} is Hermitian on $L^2_{\text{mz}}(\Gamma)$. By the definition of $\mathcal{S}f$,

$$B(v, \mathcal{S}f) = (v, f)_{L^2} = (\mathcal{S}g, f)_{L^2}. \quad (4.18)$$

Similarly, $B(\mathcal{S}f, v) = (\mathcal{S}f, g)_{L^2}$. The conjugate symmetry of B then gives that \mathcal{S} is a Hermitian operator on $L^2_{\text{mz}}(\Gamma)$.

Finally, \mathcal{S} is a negative semidefinite operator because

$$(\mathcal{S}g, g)_{L^2} = B(v, v) = - \int_{\Gamma} a \|\nabla_{\Gamma} v\|^2 \leq 0$$

for all $g \in L^2_{\text{mz}}(\Gamma)$.

By the spectral theorem for self adjoint compact operators (see [51]), assembling the above observations gives that the spectrum of \mathcal{S} is composed of a countable number of isolated negative eigenvalues and zero. \square

4.2 Elliptic problems without advection

In this section, we introduce a parametrix for (1.1) and extend the argument in Section 3 to find an integral equation form of (1.1). We will assume that a is a smooth and positive function. We shall also assume that c is a smooth complex-valued function and that (1.1) has a unique solution (see Theorems 7, 9, and 10). For the same reasons discussed in Section 2.3, if $c = 0$ we will also assume that u and f are mean-zero. We also suppose for now that $\mathbf{b} = \mathbf{0}$, and discuss the case with non-zero \mathbf{b} in the following section.

Analogous to the Laplace-Beltrami case, we let $G(r; \tilde{a}, \tilde{c})$ be the Green's function for the constant coefficient elliptic equation in the plane:

$$(\tilde{a}\Delta_2 + \tilde{c})G(r; \tilde{a}, \tilde{c}) = \delta(r), \quad (4.19)$$

where \tilde{a} and \tilde{c} are arbitrary constants.

Note that if $\tilde{c} = 0$, then the Green's function G is given by

$$G(r; \tilde{a}, \tilde{c}) = \frac{1}{2\pi\tilde{a}} \log r, \quad (4.20)$$

and if $\tilde{c} \neq 0$, then

$$G(r; \tilde{a}, \tilde{c}) = \frac{i}{4\tilde{a}} H_0^{(1)}\left(\sqrt{\tilde{c}/\tilde{a}} r\right), \quad (4.21)$$

where $H_0^{(1)}$ is the zeroth-order Hankel function of the first kind.

We use this Green's function to define a parametrix for the general variable coefficient case:

$$K(\mathbf{x}, \mathbf{x}') := G(\|\mathbf{x} - \mathbf{x}'\|; a(\mathbf{x}'), c(\mathbf{x}')), \quad (4.22)$$

for $\mathbf{x}, \mathbf{x}' \in \mathbb{R}^3$. Before proving that K is a parametrix for (1.1), however, we note that we could have chosen K to depend on the values of a and c at \mathbf{x} instead of \mathbf{x}' . We made the above choice so that $K(\mathbf{x}, \mathbf{x}')$ is defined for \mathbf{x} in a neighborhood of Γ . This allow us to apply the formula (3.13) to differentiate K .

We also note that the Green's function must have a branch cut due to the square root in the argument and logarithmic terms in the Hankel function expansions. We therefore add the assumption that c is contained in some wedge in the complex plane. In what follows, since $r = \|\mathbf{x} - \mathbf{x}'\|$ is real, we can avoid the branch cut in the Green's function by choosing the branch cut to be outside that wedge.

Since we will need them below, we note that for small $z \in \mathbb{C}$ we have the following asymptotic expansions for $H_0^{(1)}$ and its derivatives:

$$\begin{aligned} H_0^{(1)}(z) &= \frac{2i}{\pi} \log z + \mathcal{O}(1), \\ \frac{d}{dz} H_0^{(1)}(z) &= \frac{2i}{\pi z} + \mathcal{O}(z \log z), \\ \frac{d^2}{dz^2} H_0^{(1)}(z) &= -\frac{2i}{\pi z^2} + \mathcal{O}(\log z). \end{aligned} \quad (4.23)$$

We now verify that K is a candidate to be parametrix for (1.1). Afterwards, we shall prove properties of the remainder function such that K is indeed a parametrix.

Theorem 11. *The function K satisfies*

$$\nabla_\Gamma \cdot a(\mathbf{x}) \nabla_\Gamma K(\mathbf{x}, \mathbf{x}') + c(\mathbf{x}) K(\mathbf{x}, \mathbf{x}') = \delta(\mathbf{x} - \mathbf{x}') + R(\mathbf{x}, \mathbf{x}'), \quad (4.24)$$

where the derivatives are taken with respect to \mathbf{x} . Furthermore, wherever $K(\mathbf{x}, \mathbf{x}')$ is smooth the remainder function is

$$\begin{aligned} R(\mathbf{x}, \mathbf{x}') &= \nabla_\Gamma a(\mathbf{x}) \cdot \hat{\mathbf{r}} G'(r; a(\mathbf{x}'), c(\mathbf{x}')) - a(\mathbf{x}) G''(r; a(\mathbf{x}'), c(\mathbf{x}')) \frac{(\mathbf{n}(\mathbf{x}) \cdot \mathbf{r})^2}{r^2} \\ &\quad + a(\mathbf{x}) G'(r; a(\mathbf{x}'), c(\mathbf{x}')) \frac{(\mathbf{n}(\mathbf{x}) \cdot \mathbf{r})^2}{r^3} - 2a(\mathbf{x}) H(\mathbf{x}) \mathbf{n}(\mathbf{x}) \cdot \hat{\mathbf{r}} G'(r; a(\mathbf{x}'), c(\mathbf{x}')) \\ &\quad + \left(c(\mathbf{x}) - \frac{a(\mathbf{x})c(\mathbf{x}')}{a(\mathbf{x}')} \right) G(r; a(\mathbf{x}'), c(\mathbf{x}')), \end{aligned} \quad (4.25)$$

where $\mathbf{r} = \mathbf{x} - \mathbf{x}'$, $r = \|\mathbf{r}\|$, $\hat{\mathbf{r}} = \mathbf{r}/r$,

$$G'(r; a, c) = \partial_r G(r; a, c), \quad \text{and} \quad G''(r; a, c) = \partial_r^2 G(r; a, c). \quad (4.26)$$

Proof. The proof of (4.24) is exactly the same as the proof of (3.2) because of the asymptotic formula for the gradient of G , given in (4.23).

In order to verify (4.25) we assume that $K(\mathbf{x}, \mathbf{x}')$ is smooth at \mathbf{x} and compute:

$$\nabla_\Gamma \cdot a(\mathbf{x}) \nabla_\Gamma K(\mathbf{x}, \mathbf{x}') = \nabla_\Gamma a(\mathbf{x}) \cdot \nabla_\Gamma K(\mathbf{x}, \mathbf{x}') + a(\mathbf{x}) \Delta_\Gamma K(\mathbf{x}, \mathbf{x}').$$

We then use (3.13) and the fact that $\nabla_\Gamma = \nabla - \mathbf{n}(\mathbf{x})(\mathbf{n}(\mathbf{x}) \cdot \nabla)$ to find that for all $\mathbf{x} \neq \mathbf{x}'$,

$$\nabla_\Gamma \cdot a \nabla_\Gamma K = \nabla_\Gamma a \cdot \nabla K - 2aH \partial_{\mathbf{n}(\mathbf{x})} K + a(\Delta K - \partial_{\mathbf{n}(\mathbf{x})}^2 K). \quad (4.27)$$

In order to continue, we compute some derivatives of $G(r; a(\mathbf{x}'), c(\mathbf{x}'))$. If \mathbf{v} is a unit vector, then

$$\partial_{\mathbf{v}} G(r; a(\mathbf{x}'), c(\mathbf{x}')) = G'(r; a(\mathbf{x}'), c(\mathbf{x}')) \partial_{\mathbf{v}} r, \quad (4.28)$$

and

$$\partial_{\mathbf{v}}^2 G(r; a(\mathbf{x}'), c(\mathbf{x}')) = G''(r; a(\mathbf{x}'), c(\mathbf{x}')) (\partial_{\mathbf{v}} r)^2 + G'(r; a(\mathbf{x}'), c(\mathbf{x}')) \partial_{\mathbf{v}}^2 r. \quad (4.29)$$

The required derivatives of the distance function are

$$\partial_{\mathbf{v}} r = \frac{\mathbf{v} \cdot \mathbf{r}}{r} \quad \text{and} \quad \partial_{\mathbf{v}}^2 r = \frac{\mathbf{v} \cdot \mathbf{v}}{r} - \frac{(\mathbf{v} \cdot \mathbf{r})^2}{r^3}. \quad (4.30)$$

Grouping the second derivatives into the tangential Laplacian gives that

$$\begin{aligned} \Delta G(r; a(\mathbf{x}'), c(\mathbf{x}')) - \partial_{\mathbf{n}(\mathbf{x})}^2 G(r; a(\mathbf{x}'), c(\mathbf{x}')) \\ = G''(r; a(\mathbf{x}'), c(\mathbf{x}')) \left(1 - \frac{(\mathbf{n}(\mathbf{x}) \cdot \mathbf{r})^2}{r^2} \right) + G'(r; a(\mathbf{x}'), c(\mathbf{x}')) \left(\frac{1}{r} + \frac{(\mathbf{n}(\mathbf{x}) \cdot \mathbf{r})^2}{r^3} \right). \end{aligned} \quad (4.31)$$

We now note that by the definition of G , we have that

$$a(\mathbf{x}') G''(r; a(\mathbf{x}'), c(\mathbf{x}')) + \frac{a(\mathbf{x}')}{r} G'(r; a(\mathbf{x}'), c(\mathbf{x}')) + c(\mathbf{x}') G(r; a(\mathbf{x}'), c(\mathbf{x}')) = \delta(r). \quad (4.32)$$

The tangential Laplacian thus becomes

$$\begin{aligned} \Delta G(r; a(\mathbf{x}'), c(\mathbf{x}')) - \partial_{\mathbf{n}(\mathbf{x})}^2 G(r; a(\mathbf{x}'), c(\mathbf{x}')) \\ = -G''(r; a(\mathbf{x}'), c(\mathbf{x}')) \frac{(\mathbf{n}(\mathbf{x}) \cdot \mathbf{r})^2}{r^2} + \frac{(\mathbf{n}(\mathbf{x}) \cdot \mathbf{r})^2}{r^3} G'(r; a(\mathbf{x}'), c(\mathbf{x}')) \\ - \frac{c(\mathbf{x}')}{a(\mathbf{x}')} G(r; a(\mathbf{x}'), c(\mathbf{x}')) \end{aligned} \quad (4.33)$$

for all $\mathbf{x}' \neq \mathbf{x}$. If we plug (4.27) and (4.33) into (4.24), we get that $R(\mathbf{x}, \mathbf{x}')$ is given by (4.25). \square

When the coefficients a and c are constant, the remainder has a simpler form, which is clear from (4.25), and the following Hankel function identities:

$$\partial_z H_0^{(1)}(z) = -H_1^{(1)}(z) \quad \text{and} \quad \partial_z^2 H_0^{(1)}(z) - z^{-1} \partial_z H_0^{(1)}(z) = H_2^{(1)}(z). \quad (4.34)$$

Corollary 11.1. *If $a = a_0$ is a non-zero constant and c is zero, then $R(\mathbf{x}, \mathbf{x}') = R_{LB}(\mathbf{x}, \mathbf{x}')$. If $a = a_0$ and $c = c_0$ are both non-zero constants, then (4.25) becomes*

$$R(\mathbf{x}, \mathbf{x}') = -\frac{c_0}{4ia_0} H_2^{(1)}\left(\sqrt{\frac{c_0}{a_0}} r\right) \frac{(\mathbf{n}(\mathbf{x}) \cdot \mathbf{r})^2}{r^2} + \frac{\sqrt{c_0}}{2i\sqrt{a_0}} H_1^{(1)}\left(\sqrt{\frac{c_0}{a_0}} r\right) H(\mathbf{x}) \frac{\mathbf{n} \cdot \mathbf{r}}{r^2}. \quad (4.35)$$

In order to prove that an integral operator with kernel R is compact, we provide the following theorem about the behavior of the remainder term as $\mathbf{x} \rightarrow \mathbf{x}'$:

Theorem 12. *If the coefficient a is constant, then $R(\mathbf{x}, \mathbf{x}') = \mathcal{O}(1)$ as $\mathbf{x}' \rightarrow \mathbf{x}$. Otherwise, $R(\mathbf{x}, \mathbf{x}') = \mathcal{O}(\|\mathbf{x} - \mathbf{x}'\|^{-1})$ as $\mathbf{x}' \rightarrow \mathbf{x}$. The function K is therefore a parametrix in either case.*

Proof. When a is constant and c is zero, the remainder function is $R(\mathbf{x}, \mathbf{x}') = R_{LB}(\mathbf{x}, \mathbf{x}')$ and Theorem 3 gives that $R(\mathbf{x}, \mathbf{x}')$ is bounded. When c is not zero, the asymptotic formulas for the derivatives of Hankel functions and (4.25) gives that R is asymptotic to the $c = 0$ remainder as $\mathbf{x}' \rightarrow \mathbf{x}$, so the remainder has the same, bounded behaviour.

When a is not constant, we add the term $\frac{1}{a(\mathbf{x}')} \nabla_{\Gamma} a \cdot \nabla_{\Gamma} K$ to the remainder function. We may see that this term is $\mathcal{O}(r^{-1})$ through (4.28) and the asymptotic formula for the derivative of $G(z; a, c)$. The other non-regular term is

$$\left(c(\mathbf{x}) - \frac{a(\mathbf{x})c(\mathbf{x}')}{a(\mathbf{x}')} \right) G(\|\mathbf{x} - \mathbf{x}'\|; a(\mathbf{x}'), c(\mathbf{x}')),$$

which is $\mathcal{O}(r \log r)$ as $\mathbf{x}' \rightarrow \mathbf{x}$. Therefore the $\mathcal{O}(r^{-1})$ term is the dominant singularity and K is a parametrix. \square

Remark 1. *The stronger singularity when a is not constant is expected, as it is the same as is observed when the equivalent parametrix is used for the equation $\nabla \cdot a \nabla u = f$ in the plane [8].*

An example of what the remainder kernel looks like when c is real and not constant is shown in Figure 2. As we can see in the figure, if c approaches zero, then the remainder function is singular. We give the exact nature of this singularity in the following theorem, which follows directly from (4.23).

Theorem 13. *Suppose $\Gamma_c := \{\mathbf{x} \in \Gamma : c(\mathbf{x}) = 0\}$ is not empty and not all of Γ . If $\tilde{\mathbf{x}} \in \partial\Gamma_c$ and $\tilde{\mathbf{x}} \neq \mathbf{x}$, then both $K(\mathbf{x}, \mathbf{x}')$ and $R(\mathbf{x}, \mathbf{x}')$ are $\mathcal{O}(\log c(\mathbf{x}'))$ as $\mathbf{x}' \rightarrow \tilde{\mathbf{x}}$ from outside Γ_c .*

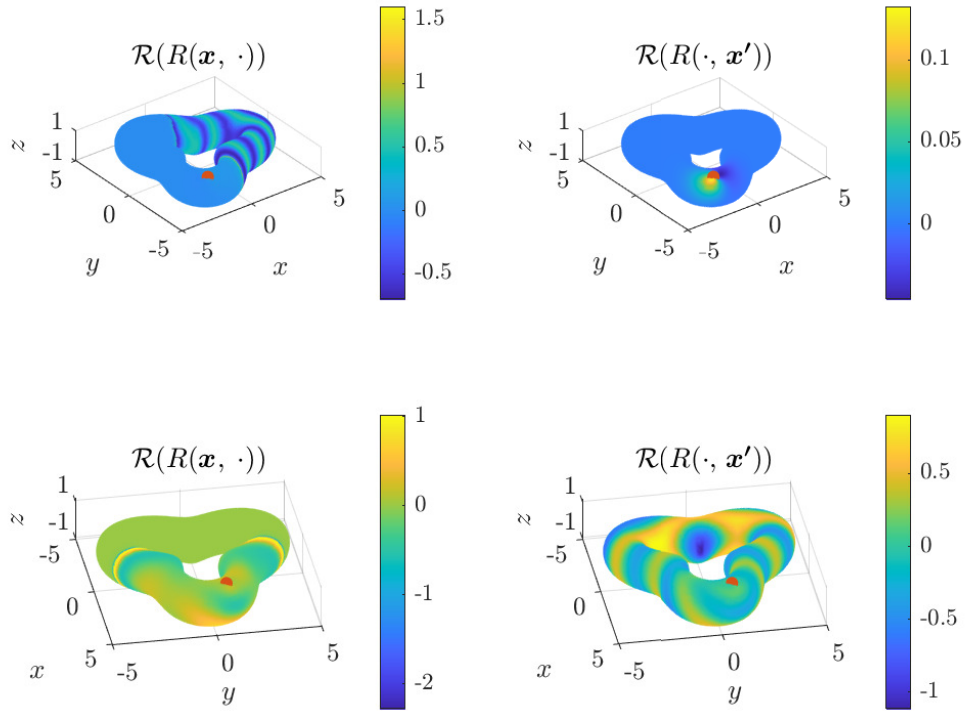


Figure 2: The figure shows the remainder kernel for an example surface PDE $c(x, y, z) = 2x$ and $a = 1$. We see that the remainder function has a singularity at points where $c(\mathbf{x}) = 0$ (the left images) and is a bounded function of \mathbf{x} (the right images). It is also clear that the remainder inherits the character of the PDE: it is oscillatory when $c > 0$ and rapidly decays when $c < 0$.

We are now ready to use our parametrix to find a second kind integral equation form of (1.1).

Theorem 14. *If a and c are smooth, then the integral equation*

$$\sigma(\mathbf{x}) + \int_{\Gamma} R(\mathbf{x}, \mathbf{x}') \sigma(\mathbf{x}') da(\mathbf{x}') = f(\mathbf{x}), \quad \text{for } \mathbf{x} \in \Gamma \quad (4.36)$$

is a second kind Fredholm integral equation on $L^2(\Gamma)$. Furthermore, if $f \in L^2(\Gamma)$ and σ is the solution of (4.36), then the function

$$u(\mathbf{x}) = \int_{\Gamma} K(\mathbf{x}, \mathbf{x}') \sigma(\mathbf{x}') da(\mathbf{x}') \quad (4.37)$$

is the unique solution of (1.1).

Proof. We begin by proving that the integral operator

$$\mathcal{R}[\sigma](\mathbf{x}) = \int_{\Gamma} R(\mathbf{x}, \mathbf{x}') \sigma(\mathbf{x}') da(\mathbf{x}') \quad (4.38)$$

is a compact map from $L^2(\Gamma)$ to itself. The remainder function has two singularities: (1) when $\mathbf{x}' \rightarrow \mathbf{x}$ and, if it is non empty, (2) when \mathbf{x}' approaches γ_c , the boundary of the subset $\Gamma_c = \{\tilde{\mathbf{x}} \in \Gamma : c(\tilde{\mathbf{x}}) = 0\}$. In order to simplify our discussion, we start by ignoring the contribution of an ϵ neighborhood of γ_c . This allows to focus on the singularity when $\mathbf{x}' \rightarrow \mathbf{x}$. What remains is an integral operator \mathcal{R}_ϵ with the kernel

$$R_\epsilon(\mathbf{x}, \mathbf{x}') := \begin{cases} R(\mathbf{x}, \mathbf{x}') & \text{dist}(\mathbf{x}', \gamma_c) > \epsilon \\ 0 & \text{otherwise} \end{cases}. \quad (4.39)$$

For any $\epsilon > 0$, R_ϵ is bounded apart from a $O(r^{-1})$ singularity at $\mathbf{x}' \approx \mathbf{x}$ (Theorem 12), so Proposition 3.11 in [29] gives that the operator \mathcal{R}_ϵ is compact on $L^2(\Gamma)$. The singularity that occurs when $c(\mathbf{x}') \rightarrow 0$ is integrable, so by the argument in the proof of Proposition 3.10 in [29], \mathcal{R} is the $L^2(\Gamma)$ -norm limit of \mathcal{R}_ϵ . The operator \mathcal{R} is therefore a compact map from $L^2(\Gamma)$ to itself. The equation (4.36) is thus a second kind Fredholm integral equation.

The proof that the u defined in (4.37) solves (1.1) is exactly the same as in Theorem 4, except that it starts from the the weak form of (1.1) :

$$\begin{aligned} B(u, \varphi) &:= \int_{\Gamma} (-a \nabla_{\Gamma} u \cdot \nabla_{\Gamma} \bar{\varphi} + c u \bar{\varphi}) \\ &= \int_{\Gamma} f \bar{\varphi}, \end{aligned} \quad (4.40)$$

for all $\varphi \in H^1(\Gamma)$. □

4.3 Elliptic problems with advection

In some cases, we wish to consider surface PDEs with a first order term, such as the semi-discretization of an advection-diffusion equation with an implicit time stepping method. In this section, we describe how the above integral equation form can easily be extended to this case, which corresponds to introducing a non-zero \mathbf{b} into (1.1).

Theorem 15. *The function K defined in (4.22) is a parametrix for (1.1) with remainder function*

$$R_{\mathbf{b}}(\mathbf{x}, \mathbf{x}') := R(\mathbf{x}, \mathbf{x}') + \mathbf{b} \cdot \nabla_{\Gamma} K(\mathbf{x}, \mathbf{x}'), \quad (4.41)$$

where the function R is defined in (4.35).

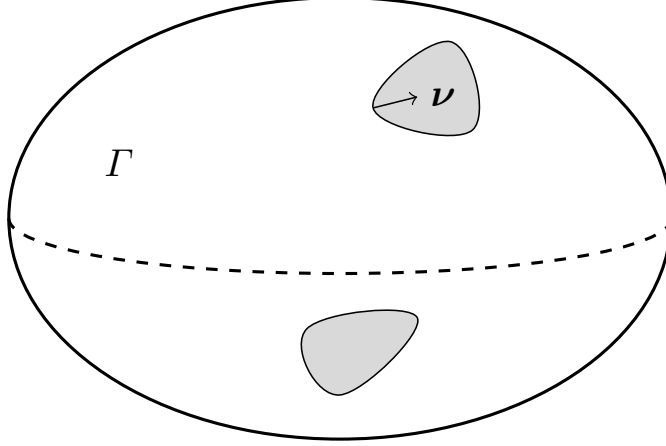


Figure 3: This figure shows an example of an open surface Γ , which is a subset of the ellipsoid $\tilde{\Gamma}$ with two patches removed. It also shows the binormal vector $\boldsymbol{\nu}$, which is normal to the $\partial\Gamma$, but tangent to Γ .

Proof. Adding a lower-order term to the equation does not change the proof of the fact that K satisfies (2.2). The advection term is additive, so (4.41) follows immediately from the definition of the remainder function. Finally, we note that the term $\mathbf{b} \cdot \nabla_{\Gamma} K$ has a singularity of $\mathcal{O}(\|\mathbf{x} - \mathbf{x}'\|^{-1})$ as $\mathbf{x}' \rightarrow \mathbf{x}$, which still allows for K to be a parametrix. \square

With the knowledge that K is a parametrix, we can use it to derive an integral equation form of (1.1) in the same manner as Theorem 14.

Theorem 16. *The integral equation*

$$\sigma(\mathbf{x}) + \int_{\Gamma} R_{\mathbf{b}}(\mathbf{x}, \mathbf{x}') \sigma(\mathbf{x}') da(\mathbf{x}') = f(\mathbf{x}), \quad \text{for } \mathbf{x} \in \Gamma, \quad (4.42)$$

is a second-kind Fredholm integral equation on $L^2(\Gamma)$. Furthermore, if $f \in L^2(\Gamma)$ and σ is the solution of (4.42), then the function u given by (4.37) is the unique solution of (1.1).

Proof. Since the additional term in $R_{\mathbf{b}}$ is not more singular than R , the integral equation (4.42) will still be second-kind. The proof of the second part follows in the same manner as in the case without advection. \square

5 Elliptic boundary value problems on surfaces

We now address the situation of surface PDEs on open surfaces with boundary conditions applied at surface edges. We suppose that Γ is an open subset of a larger closed surface $\tilde{\Gamma}$ whose boundary is comprised of smooth and non-intersecting closed curves, see Figure 3 for an example of such a surface. Throughout this section, we let $\gamma := \partial\Gamma$ be the boundary of the surface and $\boldsymbol{\nu}$ be the binormal vector to γ , i.e. the normalized vector field on γ that is defined to be tangent to Γ , perpendicular to γ , and to point away from Γ . We shall also assume that Γ does not include its boundary, and so is an open subset of $\tilde{\Gamma}$.

We start by briefly discussing the existence of solutions to such problems. We then consider problems with Neumann boundary conditions imposed at Γ , and then move on to the case where Dirichlet boundary conditions are imposed on γ .

5.1 Existence of solutions

Before we continue, we note that Theorems 7, 9, and 10 can be extended to problems on open surfaces where boundary conditions are applied on the edge γ . In order to study these in detail, we first define the trace operator, the weaker analogue of the restriction operator.

Definition 3 (Trace). Suppose \mathbf{y} is a smooth local parameterization of $\bar{\Gamma}$ and that $\gamma_{\mathbf{y}}$ is the intersection of γ and the range of \mathbf{y} . If $u \in H^1(\Gamma)$, then the trace of u is defined as

$$\mathrm{tr}_{\gamma_{\mathbf{y}}} u := \mathrm{tr}_{\mathbf{y}^{-1}(\gamma_{\mathbf{y}})}(u \circ \mathbf{y}) \circ \mathbf{y}^{-1}, \quad (5.1)$$

where $\mathrm{tr}_{\mathbf{y}^{-1}(\gamma_{\mathbf{y}})}$ is the usual trace operator for curves in \mathbb{R}^2 (see Theorem 18.1 of [52]).

By Theorem 18.1 of [52], we know that the range of the trace operator is $H^{\frac{1}{2}}(\gamma_{\mathbf{y}})$, which may be defined through the use of a parameterization and the usual one dimensional Sobolev space $H^{\frac{1}{2}}([0, L])$. To define the trace onto all of γ , we can use a partition of unity to combine the traces onto individual portions $\gamma_{\mathbf{y}_i}$. For this to be well defined, we must show that the trace is parameterization-independent.

Theorem 17. The operator $\mathrm{tr}_{\gamma_{\mathbf{y}}}$ is independent of the local parameterization used in its definition.

Proof. Let \mathbf{y} and \mathbf{z} be two smooth local parameterizations that map the domains U and V onto $\tilde{\Gamma} \subset \bar{\Gamma}$, and such that $\gamma_{\mathbf{y}} = \gamma_{\mathbf{z}}$. We begin by showing that $C^\infty(\tilde{\Gamma})$ is dense in $H^1(\tilde{\Gamma})$. By the definitions of the surface gradient and $H^1(\tilde{\Gamma})$, we have that

$$\begin{aligned} H^1(\tilde{\Gamma}) &= \{f \in L^2(\tilde{\Gamma}) \mid f \circ \mathbf{y} \in H^1(U)\}, \\ C^\infty(\tilde{\Gamma}) &= \{f \in C(\tilde{\Gamma}) \mid f \circ \mathbf{y} \in C^\infty(U)\}. \end{aligned} \quad (5.2)$$

Standard density results in the plane then imply that $C^\infty(\tilde{\Gamma})$ is dense in $H^1(\tilde{\Gamma})$, see [28].

Next, we note that if $v \in C^\infty(\tilde{\Gamma})$, then

$$\mathrm{tr}_{\mathbf{y}^{-1}(\gamma_{\mathbf{y}})}(v \circ \mathbf{y}) \circ \mathbf{y}^{-1} = \mathrm{tr}_{\mathbf{z}^{-1}(\gamma_{\mathbf{z}})}(v \circ \mathbf{z}) \circ \mathbf{z}^{-1}, \quad (5.3)$$

and therefore $\mathrm{tr}_{\gamma_{\mathbf{y}}} v$ is independent of the smooth local parameterization used in its definition. The density of $C^\infty(\tilde{\Gamma})$ then implies that the trace operator is independent of the local parameterization. \square

With this theorem, we can extend our definition of the trace onto the whole of γ . Further, by choosing a standard set of parameterizations, it is clear that the trace operator maps $H^1(\Gamma)$ to $H^{\frac{1}{2}}(\gamma) \subset L^2(\gamma)$.

With the trace defined, we are now ready to prove the well-posedness of some boundary value problems along surfaces. When the Neumann boundary conditions

$$\boldsymbol{\nu} \cdot \nabla_{\Gamma} u|_{\gamma} = f_{\gamma} \quad (5.4)$$

are applied, the proofs of the above existence results, Theorems 7, 9, and 10, are the same except that the conjugate linear form is replaced by

$$L(\rho) := \int_{\Gamma} \bar{\rho} f + \int_{\gamma} \bar{\rho} f_{\gamma}. \quad (5.5)$$

This conjugate linear form is still bounded on $H^1(\Gamma)$ because the trace operator is bounded.

We now consider the case where Dirichlet boundary conditions

$$u|_{\gamma} = f_{\gamma}, \quad (5.6)$$

are applied. The proofs for when $h = 0$ are the same as the case without boundaries, except that u to must be restricted to live in the subspace of trace-zero functions. For the inhomogeneous case, we must first show that for any $f_{\gamma} \in C^1(\gamma)$, there exists a $u_{f_{\gamma}} \in H^1(\Gamma)$, whose trace is f_{γ} .

To see that $u_{f_{\gamma}}$ exists, let $\Pi(\mathbf{x})$ be the point on γ closest to \mathbf{x} in the Euclidean norm and let $\epsilon(\Pi(\mathbf{x}))$ be a distance such that if $\mathrm{dist}(\mathbf{x}, \gamma) < \epsilon(\Pi(\mathbf{x}))$, then $\Pi(\mathbf{x})$ is unique. Finally, let $\eta(r)$

be a smooth function on $[0, \infty)$ that is 1 at $r = 0$ and that is identically zero for $r > 1$. A suitable choice of u_{f_γ} can be written as

$$u_{f_\gamma}(\mathbf{x}) = f_\gamma(\Pi(\mathbf{x})) \eta \left(\frac{\|\mathbf{x} - \Pi(\mathbf{x})\|^2}{\epsilon(\Pi(\mathbf{x}))^2} \right).$$

This function will be continuously differentiable on the closure of Γ because the surface is smooth and $\Pi(\mathbf{x})$ will vary smoothly on the support of u . This will be enough to guarantee that $u_{f_\gamma} \in H^1(\Gamma)$. By the linearity of (1.1) and (5.29), we can then apply the analogues of Theorems 7, 9, and 10 to $u - u_{f_\gamma}$ and see that the solution exists if and only if it exists in the case where $f_\gamma = 0$.

5.2 Neumann boundary conditions

In this section, we derive an integral equation supposing that Neumann boundary conditions are imposed on γ :

$$\boldsymbol{\nu} \cdot \nabla_\Gamma u|_\gamma = f_\gamma, \quad (5.7)$$

where f_γ is given data. Our goal in this section will be to use the parametrization (4.22) to convert equations (1.1) and (5.7) into a system of integral equations.

In order to enforce the boundary conditions, we must include a boundary term in our representation of the solution u . The new augmented representation is

$$u = \mathcal{K}_\Gamma[\sigma] + \mathcal{K}_\gamma[\mu], \quad (5.8)$$

where \mathcal{K}_Γ is the surface operator

$$\mathcal{K}_\Gamma[\sigma](\mathbf{x}) := \int_\Gamma K(\mathbf{x}, \mathbf{x}') \sigma(\mathbf{x}') da(\mathbf{x}'), \quad \forall \mathbf{x} \in \Gamma \quad (5.9)$$

and \mathcal{K}_γ is the edge operator

$$\mathcal{K}_\gamma[\mu](\mathbf{x}) := \int_\gamma K(\mathbf{x}, \mathbf{x}') \mu(\mathbf{x}') ds(\mathbf{x}'), \quad \forall \mathbf{x} \in \Gamma. \quad (5.10)$$

The following lemma gives how the differential operator in (1.1) acts on this representation.

Lemma 1. *If u is given by (5.8), $\sigma \in L^2(\Gamma)$, and $\mu \in L^2(\gamma)$, then*

$$\nabla_\Gamma \cdot a \nabla_\Gamma u + \mathbf{b} \cdot \nabla_\Gamma u + cu = \sigma + \mathcal{R}_\Gamma[\sigma] + \mathcal{R}_\gamma[\mu], \quad (5.11)$$

in the interior of Γ , where

$$\begin{aligned} \mathcal{R}_\Gamma[\sigma](\mathbf{x}) &:= \int_\Gamma R(\mathbf{x}, \mathbf{x}') \sigma(\mathbf{x}') da(\mathbf{x}'), \\ \mathcal{R}_\gamma[\mu](\mathbf{x}) &:= \int_\gamma R(\mathbf{x}, \mathbf{x}') \mu(\mathbf{x}') ds(\mathbf{x}'), \quad \text{for all } \mathbf{x} \in \Gamma. \end{aligned} \quad (5.12)$$

Proof. We note that

$$\mathcal{K}_\Gamma[\sigma](\mathbf{x}) = \int_{\tilde{\Gamma}} K(\mathbf{x}, \mathbf{x}') \tilde{\sigma}(\mathbf{x}') da(\mathbf{x}'),$$

where $\tilde{\sigma}$ is the zero-extension of σ to the rest of $\tilde{\Gamma}$. Theorem 14 thus gives the first two terms of (5.11). For the other term, we note that since each $\mathbf{x} \in \Gamma$ is a finite distance away from γ , the kernel of \mathcal{K}_γ is smooth in a neighborhood of \mathbf{x} and we may simply pull the derivative inside the integral. \square

To enforce the boundary conditions, we need the following two lemmas.

Lemma 2. *If $\sigma \in L^2(\Gamma)$, then $\mathcal{K}_\Gamma[\sigma] \in H^2(\Gamma)$. Further, if $\sigma \in L^\infty(\Gamma)$ then*

$$\lim_{\mathbf{x} \rightarrow \tilde{\mathbf{x}} \in \gamma} \boldsymbol{\nu}(\tilde{\mathbf{x}}) \cdot \nabla_\Gamma \mathcal{K}_\Gamma[\sigma](\mathbf{x}) = \int_\Gamma \boldsymbol{\nu}(\tilde{\mathbf{x}}) \cdot \nabla_\Gamma K(\mathbf{x}, \mathbf{x}') \sigma(\mathbf{x}') da(\mathbf{x}'). \quad (5.13)$$

Proof. By the previous lemma, it is clear that $(\nabla_\Gamma \cdot a \nabla_\Gamma + \mathbf{b} \cdot \nabla_\Gamma + c) \mathcal{K}_\Gamma[\sigma] \in L^2(\Gamma)$. Theorem 6.30 of [73] then gives that $\mathcal{K}_\Gamma[\sigma] \in H^2(\Gamma)$.

To compute the gradient of K_Γ , we extend our integral operators to be defined on $\tilde{\Gamma}$ by extending σ by zero. We can then repeat the argument used in the proof of Theorem 4 to find that

$$\nabla_\Gamma \mathcal{K}_\Gamma[\sigma](\mathbf{x}) = \int_\Gamma \int_\Gamma \nabla_\Gamma K(\mathbf{x}, \mathbf{x}') \sigma(\mathbf{x}') da(\mathbf{x}'). \quad (5.14)$$

We now assume that σ is in $L^\infty(\Gamma)$. Proposition 3.12 in [29] applied on $\tilde{\Gamma}$ gives that $\nabla_\Gamma \mathcal{K}_\Gamma[\sigma]$ is a continuous vector field on $\tilde{\Gamma}$, and so the limit can simply be evaluated. Dotting the limiting value with $\boldsymbol{\nu}(\tilde{\mathbf{x}})$ gives (5.13). \square

Lemma 3. *If $\mu \in C(\gamma)$, then*

$$\lim_{\mathbf{x} \rightarrow \tilde{\mathbf{x}} \in \gamma} \boldsymbol{\nu}(\tilde{\mathbf{x}}) \cdot \nabla_\Gamma \mathcal{K}_\gamma[\mu] = -\frac{1}{2a(\tilde{\mathbf{x}})} \mu(\tilde{\mathbf{x}}) + \mathcal{K}'_\gamma[\mu](\tilde{\mathbf{x}}) \quad (5.15)$$

for all $\tilde{\mathbf{x}} \in \gamma$, where

$$\mathcal{K}'_\gamma[\mu](\mathbf{x}) = \int_\gamma \boldsymbol{\nu}(\mathbf{x}) \cdot \nabla_\Gamma K(\mathbf{x}, \mathbf{x}')(\mathbf{x}') ds(\mathbf{x}'), \quad \text{for all } \mathbf{x} \in \gamma. \quad (5.16)$$

Proof. We begin by showing (5.15) in the Laplace-Beltrami case.

Let $\mathbf{y} = \mathbf{y}(s, t)$ be a smooth parameterization of Γ with domain $V \subset \mathbb{R}^2$ such that Γ_V , the range of \mathbf{y} , contains the point $\tilde{\mathbf{x}}$. Also let $\tilde{\boldsymbol{\nu}} = \boldsymbol{\nu}(\tilde{\mathbf{x}})$. We shall consider the limit

$$\lim_{\substack{\mathbf{x} \rightarrow \tilde{\mathbf{x}} \\ \mathbf{x} \in \Gamma \setminus \gamma}} \tilde{\boldsymbol{\nu}} \cdot \nabla_\Gamma \mathcal{K}_\gamma[\mu \chi_{\Gamma_V}](\mathbf{x}), \quad (5.17)$$

where χ_{Γ_V} is the characteristic function for Γ_V . The limit of the remaining part,

$$\lim_{\substack{\mathbf{x} \rightarrow \tilde{\mathbf{x}} \\ \mathbf{x} \in \Gamma \setminus \gamma}} \tilde{\boldsymbol{\nu}} \cdot \nabla_\Gamma \mathcal{K}_\gamma[\mu(1 - \chi_{\Gamma_V})](\mathbf{x}), \quad (5.18)$$

may easily be computed by the dominated convergence theorem, since the kernel of K_γ is smooth for $\mathbf{x} \in \Gamma \setminus \Gamma_V$.

Without loss of generality, we shall also suppose that \mathbf{y} maps $(0, 0)$ to $\tilde{\mathbf{x}}$ and maps the line segment $[-L, L] \times \{0\}$ to $\gamma \cap \Gamma_V$. Under this parameterization, the integral becomes

$$\tilde{\boldsymbol{\nu}} \cdot \nabla_\Gamma \mathcal{K}_\gamma[\mu \chi_{\Gamma_V}](\mathbf{x}) = \frac{1}{2\pi} \int_{-L}^L \frac{\tilde{\boldsymbol{\nu}} \cdot (\mathbf{x} - \mathbf{y}(s, 0))}{\|\mathbf{x} - \mathbf{y}(s, 0)\|^2} \mu(\mathbf{y}(s, 0)) \sqrt{g_{ss}} ds. \quad (5.19)$$

We consider test points \mathbf{x} that approach $\mathbf{y}(0, 0)$ along the curve $\mathbf{y}(ah, bh)$ and Taylor expand the kernel of $\tilde{\boldsymbol{\nu}} \cdot \nabla_\Gamma \mathcal{K}_\gamma$ in the vicinity of $(0, 0)$:

$$\begin{aligned} & \frac{1}{2\pi} \frac{\tilde{\boldsymbol{\nu}} \cdot (\mathbf{y}(ah, bh) - \mathbf{y}(s, 0))}{\|\mathbf{y}(ah, bh) - \mathbf{y}(s, 0)\|^2} \sqrt{g_{ss}(s, t)} \\ &= \frac{1}{2\pi} \frac{(\tilde{\boldsymbol{\nu}} \cdot \nabla \mathbf{y}(0, 0)) \cdot (ah - s, bh) + \mathcal{O}(h^2 + s^2)}{(ah - s, bh)^T \nabla \mathbf{y}(0, 0)^T \nabla \mathbf{y}(0, 0) (ah - s, bh) + \mathcal{O}(h^3 + s^3)} \left(\sqrt{g_{ss}(0, 0)} + \mathcal{O}(s) \right). \end{aligned} \quad (5.20)$$

We now note that $\tilde{\nu} = -g_{ss}^{-1}(0,0)^{-1/2} \nabla \mathbf{y}(0,0) g^{-1}(0,0) \hat{e}_t$, where $\hat{e}_t \in \mathbb{R}^2$ is the standard basis vector in the t direction. We thus have that $\tilde{\nu} \cdot \nabla \mathbf{y} = -g_{ss}^{-1} \hat{e}_t$, so the kernel (5.20) can thus be written as

$$\begin{aligned} & \frac{1}{2\pi} \frac{\tilde{\nu} \cdot (\mathbf{y}(ah, bh) - \mathbf{y}(s, 0))}{\|\mathbf{y}(ah, bh) - \mathbf{y}(s, 0)\|^2} \sqrt{g_{ss}(s, t)} \\ &= \frac{-1}{2\pi} \sqrt{\frac{g_{ss}(0, 0)}{g_{tt}^{-1}(0, 0)}} \frac{bh}{(ah - s, bh)^T g(0, 0) (ah - s, bh)} + k_b(s, h), \end{aligned} \quad (5.21)$$

where $k_b(s, h) = \mathcal{O}(1)$ as $s, h \rightarrow 0$ because g is positive definite.

To examine the limit as $h \rightarrow 0$, we split the kernel into two parts: the singular part, $k_s(s, h)$ and the bounded part $k_b(s, h)$. Expanding the denominator of k_s gives that

$$k_s(s, h) = \frac{-1}{2\pi} \sqrt{\frac{g_{ss}}{g_{tt}^{-1}}} \frac{bh}{(ah - s)^2 g_{ss} + 2bh(ah - s)g_{st} + b^2 h^2 g_{tt}},$$

where the metric g is evaluated at $(0, 0)$. Substituting $\tilde{h} = b\sqrt{g_{tt}/g_{ss}}h$, gives the slightly nicer expression

$$k_s(s, h) = \frac{-1}{2\pi} \frac{1}{\sqrt{g_{tt}(g^{-1})_{ss}}} \frac{\tilde{h}}{\left(\frac{a}{b} \sqrt{\frac{g_{ss}}{g_{tt}}} \tilde{h} - s\right)^2 + 2\tilde{h} \left(\frac{a}{b} \sqrt{\frac{g_{ss}}{g_{tt}}} \tilde{h} - s\right) \frac{g_{st}}{\sqrt{g_{ss}g_{tt}}} + \tilde{h}^2}.$$

Since $\tilde{h} > 0$ we can analytically compute

$$\begin{aligned} \int_{-L}^L k_s(s, h) ds &= \int_{-\infty}^{\infty} k_s(s, h) ds - \int_{\mathbb{R} \setminus [-L, L]} k_s(s, h) ds \\ &= \frac{-1}{2\pi} \frac{1}{\sqrt{g_{tt} \frac{g_{ss}}{g_{ss}g_{tt} - g_{st}^2}}} \frac{2\pi}{\sqrt{4 - \frac{4g_{st}^2}{g_{ss}g_{tt}}}} - \int_{\mathbb{R} \setminus [-L, L]} k_s(s, h) ds \\ &= -\frac{1}{2} - \int_{\mathbb{R} \setminus [-L, L]} k_s(s, h) ds. \end{aligned}$$

Since

$$k_s(s, h) \sim \frac{-1}{2\pi} \frac{1}{\sqrt{g_{tt}(g^{-1})_{tt}}} \frac{\tilde{h}}{s^2} \quad (5.22)$$

for s larger than \tilde{h} , the dominated convergence theorem gives that

$$\lim_{h \rightarrow 0^+} \int_{-L}^L k_s(s, h) ds = -\frac{1}{2}.$$

We now compute the integral with a Lipschitz continuous density μ :

$$\begin{aligned} \lim_{h \rightarrow 0^+} \int_{-L}^L k_s(s, h) \mu(\mathbf{x}(s, 0)) ds &= \lim_{h \rightarrow 0^+} \int_{-L}^L k_s(s, h) (\mu(\mathbf{x}(s, 0)) - \mu(\tilde{\mathbf{x}})) ds \\ &\quad + \lim_{h \rightarrow 0^+} \int_{-L}^L k_s(s, h) \mu(\tilde{\mathbf{x}}) ds \\ &= \lim_{h \rightarrow 0^+} \int_{-L}^L k_s(s, h) (\mu(\mathbf{x}(s, 0)) - \mu(\tilde{\mathbf{x}})) ds - \frac{\mu(\tilde{\mathbf{x}})}{2}. \end{aligned}$$

Since μ is Lipschitz continuous, we can apply the dominated convergence theorem provided $k_s(s, h)s$ is bounded. Clearly, $k_s(s, h)s$ is a rational function with a second order zero at $(0, 0)$ in the numerator and denominator (since g is positive definite). It is thus a bounded function of s, h . We may use the dominated convergence theorem and the fact that $k_s(s, 0) = 0$ to see that

$$\lim_{h \rightarrow 0^+} \int_{-L}^L k_s(s, h) \mu(\mathbf{x}(s, 0)) du = -\frac{\mu(\tilde{\mathbf{x}})}{2}. \quad (5.23)$$

For the contribution of $k_b(s, h)$, we note that, since $k_b(s, h) = \mathcal{O}(1)$ as $h \rightarrow 0$, we may use the dominated convergence theorem to conclude that

$$\begin{aligned} \lim_{\mathbf{y} \rightarrow \tilde{\mathbf{x}}} \partial_{\tilde{\mathbf{v}}} \mathcal{K}_\gamma[\mu \chi_{\Gamma_V}](\mathbf{x}) &= -\frac{1}{2} \mu(\mathbf{y}(0, 0)) + \int_{-L}^L \frac{\tilde{\mathbf{v}} \cdot (\mathbf{y}(0, 0) - \mathbf{y}(s, 0))}{\|\mathbf{y}(0, 0) - \mathbf{y}(s, 0)\|^2} \mu(\mathbf{y}(s, 0)) \sqrt{g_{ss}} ds \\ &= -\frac{1}{2} \mu(\tilde{\mathbf{x}}) + \mathcal{K}'_\gamma[\mu \chi_{\Gamma_V}](\tilde{\mathbf{x}}). \end{aligned} \quad (5.24)$$

The above argument also applies to the case when $c \neq 0$ because the parametrix has the same singularity as in the Laplace-Beltrami case. Since introducing an $a \neq 1$ divides the parametrix by that a and neither a nor \mathbf{b} change the singularity, we have (5.15).

Finally, we note that since the kernel of \mathcal{K}'_γ is bounded, Proposition 3.10 in [29] gives that \mathcal{K}'_γ is bounded on $L^\infty(\gamma)$. The density of Lipschitz continuous functions then shows that (5.15) holds for all continuous μ . \square

Combining the above two lemmas gives the following theorem.

Theorem 18. *If u is given by (5.8), $\sigma \in L^\infty(\Gamma)$, and $\mu \in C(\gamma)$, then*

$$\boldsymbol{\nu} \cdot \nabla_\Gamma u|_\gamma = -\frac{1}{2a} \mu + \mathcal{K}'_\Gamma[\sigma] + \mathcal{K}'_\gamma[\mu], \quad (5.25)$$

where

$$\mathcal{K}'_\Gamma[\sigma](\mathbf{x}) := \int_\Gamma \boldsymbol{\nu}(\mathbf{x}) \cdot \nabla_\Gamma K(\mathbf{x}, \mathbf{x}') \sigma(\mathbf{x}'), \quad \text{for all } \mathbf{x} \in \gamma. \quad (5.26)$$

In order to verify that our final integral equations are Fredholm second kind, we now show that the integral operators in equations (5.11) and (5.25) are compact in L^2 .

Theorem 19. *The following operators are compact from L^2 to L^2 :*

$$\mathcal{K}_\Gamma, \quad \mathcal{K}'_\Gamma, \quad \mathcal{R}_\Gamma, \quad \mathcal{K}_\gamma, \quad \mathcal{K}'_\gamma, \quad \text{and} \quad \mathcal{R}_\gamma.$$

Proof. The operators \mathcal{K}_Γ , \mathcal{K}_γ , and \mathcal{R}_γ are compact because they are Hilbert-Schmidt maps on their respective domains and ranges (see Proposition 0.45 in [29]). The operator \mathcal{K}'_γ is a compact map from $L^2(\gamma)$ to itself by Proposition 3.11 in [29]. The operator \mathcal{R}_Γ is a compact from $L^2(\Gamma)$ to itself by Theorem 14.

Finally, we note that $\mathcal{K}'_\Gamma := \boldsymbol{\nu} \cdot \text{trace} \nabla_\Gamma \mathcal{K}_\Gamma$ with $\mathcal{K}' : L^2(\Gamma) \rightarrow H^{\frac{1}{2}}(\Gamma)$ because

$$\begin{aligned} \mathcal{K}_\Gamma &: L^2(\Gamma) \rightarrow H^2(\Gamma), \\ \nabla_\Gamma &: H^2(\Gamma) \rightarrow (H^1(\Gamma))^3, \\ \boldsymbol{\nu} \cdot \text{trace} &: (H^1(\Gamma))^3 \rightarrow H^{\frac{1}{2}}(\gamma). \end{aligned}$$

The compact embedding of $H^{\frac{1}{2}}(\gamma)$ into $L^2(\gamma)$ then gives that \mathcal{K}'_Γ is a compact from $L^2(\Gamma)$ to $L^2(\gamma)$. \square

Assembling Lemma 1 and Theorems 18 and 19 gives the following theorem.

Theorem 20. *If $\sigma \in L^\infty(\Gamma)$, $\mu \in C(\gamma)$, and they solve the Fredholm second kind system of equations*

$$\begin{aligned} \sigma + \mathcal{R}_\Gamma[\sigma] + \mathcal{R}_\gamma[\mu] &= f, \\ -\frac{1}{2a} \mu + \mathcal{K}'_\Gamma[\sigma] + \mathcal{K}'_\gamma[\mu] &= f_\gamma \end{aligned} \quad (5.27)$$

then

$$u = \mathcal{K}_\Gamma[\sigma] + \mathcal{K}_\gamma[\mu], \quad (5.28)$$

is the solution of (1.1) with boundary condition (5.7).

We conclude this section by noting that the kernel of \mathcal{K}'_γ is smooth, which will allow us to efficiently discretize it using the trapezoid rule.

Theorem 21. *The kernel of \mathcal{K}'_γ is smooth.*

The proof of this fact is identical to the proof that the adjoint of the Laplacian double-layer potential operator in the plane is smooth when the target point is on the boundary curve, see Section 11.1 of [43].

5.3 Dirichlet boundary conditions

We now wish to consider the case where Dirichlet boundary conditions are applied on γ :

$$u|_\gamma = f_\gamma, \quad (5.29)$$

where f_γ is given data. In order to enforce the Dirichlet boundary conditions, we shall use the representation

$$u = \mathcal{K}_\Gamma[\sigma] + \mathcal{N}_\gamma[\mu], \quad (5.30)$$

where \mathcal{K}_Γ is the same as in the previous section and \mathcal{N}_γ is the edge operator

$$\mathcal{N}_\gamma[\mu](\mathbf{x}) := \int_\gamma \boldsymbol{\nu}(\mathbf{x}') \cdot \nabla'_\Gamma K(\mathbf{x}, \mathbf{x}') \mu(\mathbf{x}') ds(\mathbf{x}'), \quad \text{for all } \mathbf{x} \in \Gamma. \quad (5.31)$$

The kernel of \mathcal{N}_γ is smooth because it has the same behaviour when $\mathbf{x} \approx \mathbf{x}'$ as the kernel of \mathcal{K}'_γ .

The following lemma gives how the differential operator acts on this representation:

Lemma 4. *If u is given by (5.30), $\sigma \in L^2(\Gamma)$, $\|\mathbf{b}\| < \infty$, and $\mu \in L^2(\gamma)$, then*

$$\nabla_\Gamma \cdot a \nabla_\Gamma u + \mathbf{b} \cdot \nabla_\Gamma u + c u = \sigma + \mathcal{R}_\Gamma[\sigma] + \mathcal{T}_\gamma[\mu], \quad (5.32)$$

in the interior of Γ , where

$$\mathcal{T}_\gamma[\mu](\mathbf{x}) := \int_\gamma \boldsymbol{\nu}(\mathbf{x}') \cdot \nabla'_\Gamma R(\mathbf{x}, \mathbf{x}') \mu(\mathbf{x}') ds(\mathbf{x}'), \quad \text{for all } \mathbf{x} \in \Gamma. \quad (5.33)$$

Proof. The proof is the same as the proof of Lemma 1. □

In order to enforce the boundary conditions, we need the following theorem, whose proof is very similar to the proof of Theorem 18.

Theorem 22. *If u is given by (5.30), $\sigma \in L^2(\Gamma)$, and $\mu \in C(\gamma)$, then along the boundary γ we have that:*

$$u|_\gamma = -\frac{1}{2a}\mu + \mathcal{K}_\Gamma[\sigma] + \mathcal{N}_\gamma[\mu], \quad (5.34)$$

where for $\mathbf{x} \in \gamma$

$$\begin{aligned} \mathcal{K}_\Gamma[\sigma](\mathbf{x}) &:= \int_\Gamma K(\mathbf{x}, \mathbf{x}') \sigma(\mathbf{x}') da(\mathbf{x}'), \\ \mathcal{N}_\gamma[\mu](\mathbf{x}) &:= \int_\gamma \boldsymbol{\nu}(\mathbf{x}') \cdot \nabla'_\Gamma K(\mathbf{x}, \mathbf{x}') \mu(\mathbf{x}') ds(\mathbf{x}'). \end{aligned} \quad (5.35)$$

As before, we consider the compactness of our new integral operators.

Theorem 23. *The operators \mathcal{K}_Γ and \mathcal{N}_γ are compact from L^2 to L^2 . The operator \mathcal{T}_γ is a compact map from $L^2(\gamma) \rightarrow L^2(\Gamma)$ if a is constant, $\mathbf{b} = \mathbf{0}$, and c is either identically zero or bounded away from zero.*

Proof. The operators \mathcal{K}_Γ and \mathcal{N}_γ may be seen to be compact through Proposition 3.11 in [29].

We now prove that \mathcal{T}_γ is compact in the Laplace-Beltrami case by proving that its adjoint, $\boldsymbol{\nu} \cdot \text{trace } \nabla_\Gamma(\mathcal{R}_\Gamma)^*$, is a compact map from $L^2(\Gamma)$ to $L^2(\gamma)$. Since $\boldsymbol{\nu}$ is smooth, it is enough to show that the operator $\text{trace } \mathbf{e}_j \cdot \nabla_\Gamma(\mathcal{R}_\Gamma)^*$ is compact for each of the standard three dimensional basis vectors \mathbf{e}_j .

The kernel of the operator $\text{trace } \mathbf{e}_j \cdot \nabla_\Gamma(\mathcal{R}_\Gamma)^*$ is

$$\begin{aligned} k(\mathbf{x}, \mathbf{x}') &:= \mathbf{e}_j \cdot \nabla'_\Gamma R_{\text{LB}}(\mathbf{x}, \mathbf{x}') \\ &= \mathbf{e}_j \cdot \nabla'_\Gamma \frac{1}{\pi} \left(\frac{\mathbf{n}(\mathbf{x}) \cdot (\mathbf{r})}{r^2} \right)^2 - \frac{H(\mathbf{x})}{\pi} \mathbf{e}_j \cdot \nabla'_\Gamma \frac{\mathbf{n}(\mathbf{x}) \cdot (\mathbf{r})}{r^2}. \end{aligned} \quad (5.36)$$

The second term in the expression can be expanded as

$$\mathbf{e}_j \cdot \nabla'_\Gamma \frac{\mathbf{n}(\mathbf{x}) \cdot (\mathbf{r})}{r^2} = -\frac{\mathbf{e}_j \cdot [\mathbf{n}(\mathbf{x}) - (\mathbf{n}(\mathbf{x}') \cdot \mathbf{n}(\mathbf{x}))\mathbf{n}(\mathbf{x}')] }{r^2} + 2\frac{\mathbf{n}(\mathbf{x}) \cdot (\mathbf{r})\mathbf{e}_j \cdot (\mathbf{r})}{r^4}, \quad (5.37)$$

which has an $\mathcal{O}(r^{-1})$ singularity as $\mathbf{x} \rightarrow \mathbf{x}'$. The first term in (5.36) has the same singularity by the chain rule. We therefore have that

$$k(\mathbf{x}, \mathbf{x}') = \frac{q(\mathbf{x}, \mathbf{x}')}{r}, \quad (5.38)$$

where $q(\mathbf{x}, \mathbf{x}')$ is a bounded function on $\Gamma \times \Gamma \setminus \{\mathbf{x} = \mathbf{x}'\}$. Lemma 3.4 and Theorem 4.1 from [64] therefore give that $\mathbf{e}_j \cdot \nabla_\Gamma(\mathcal{R}_\Gamma)^*$ is a bounded map from $L^2(\Gamma)$ to $H^{1-\epsilon}(\Gamma)$.

Composing with the trace map sends the result from $H^{1-\epsilon}(\Gamma)$ to $H^{\frac{1}{2}-\epsilon}(\gamma)$. Since $H^{\frac{1}{2}-\epsilon}(\gamma)$ is compactly embedded in $L^2(\gamma)$, we have that $\text{trace } \mathbf{e}_j \cdot \nabla_\Gamma(\mathcal{R}_\Gamma)^*$ is a compact map from $L^2(\Gamma)$ to $L^2(\gamma)$. Multiplying by the smooth function $\boldsymbol{\nu} \cdot \mathbf{e}_j$ and summing over j preserves compactness, and therefore we have that \mathcal{T}_γ^* is compact from $L^2(\Gamma)$ to $L^2(\gamma)$. We thus have that \mathcal{T}_γ is a compact map from $L^2(\gamma)$ to $L^2(\Gamma)$.

Moving to the Helmholtz-Beltrami case ($c \neq 0$), does not change the singularity of the kernels involved and so will the above argument can be used to show that \mathcal{T}_γ is still compact. Finally, setting a to be any constant only divides the parametrix and it's argument by that constant, so does not change the compactness. \square

Assembling the above lemmas gives the following theorem.

Theorem 24. *If $\sigma \in L^\infty(\Gamma)$, $\mu \in C(\gamma)$, and they solve the Fredholm second kind system of equations*

$$\begin{aligned} \sigma + \mathcal{R}_\Gamma[\sigma] + \mathcal{T}_\gamma[\mu] &= f, \\ -\frac{1}{2a}\mu + \mathcal{N}_\Gamma[\sigma] + \mathcal{K}'_\gamma[\mu] &= f_\gamma \end{aligned} \quad (5.39)$$

then

$$u = \mathcal{K}_\Gamma[\sigma] + \mathcal{N}_\gamma[\mu], \quad (5.40)$$

is the solution of (1.1) with boundary condition (5.29).

Remark 2. *If γ can be split into two disjoint edges, γ_N and γ_D , then we can solve (1.1) with Neumann boundary conditions applied on γ_N and Dirichlet boundary conditions applied on γ_D . This could be done by representing the solution as*

$$u = \mathcal{K}_\Gamma[\sigma] + \mathcal{K}_{\gamma_N}[\mu] + \mathcal{N}_{\gamma_D}[\rho] \quad (5.41)$$

and applying the above identities to derive a system of coupled integral equations that enforce (1.1) and the boundary conditions.

6 A numerical solver

In this section, we present a numerical method for discretizing (4.36) and using it to find the solution of (1.1) on any smooth surface without boundary. In short, equation (4.36) is discretized using a Nyström-like method based on the one described in [11], resulting in a finite dimensional linear system whose solution is a vector of approximate point-values of the function σ . The linear system to be solved is dense, and we use a modified version of the *Fast Linear Algebra in MATLAB* (*FLAM*) software library [41] to accelerate the its solution via fast matrix-vector applications coupled with GMRES [68]. In the following subsections, we provide some additional detail regarding the quadratures and matrix compression techniques used in solving the linear system. Finally, we end with a discussion on how to discretize (5.27) and (5.39) and use them to find the solution of (1.1) on surfaces with boundaries.

6.1 Nyström discretization

In order to discretize integral equation (4.36) along a surface Γ , we first need a description of the surface itself. The surface Γ is assumed to be specified by a collection of M non-overlapping curvilinear triangles Γ_i so that $\Gamma = \cup_i \Gamma_i$. Each Γ_i is parameterized by a function \mathbf{y}_i which maps the standard simplex triangle T_0 to $\Gamma_i \subset \mathbb{R}^3$, where T_0 is given by

$$T_0 = \{(u, v) \in \mathbb{R}^2 \mid u, v \geq 0 \text{ and } u \leq 1 - v\}. \quad (6.1)$$

The integral equation along Γ is then divided into several pieces, each over T_0 :

$$\sigma(\mathbf{x}) + \sum_{i=1}^M \int_{T_0} R(\mathbf{x}, \mathbf{y}_i(u, v)) \sigma(\mathbf{y}_i(u, v)) da(\mathbf{y}_i(u, v)) = f(\mathbf{x}), \quad \text{for } \mathbf{x} \in \Gamma. \quad (6.2)$$

In a pure Nyström discretization, the above integral equation is transformed into a finite dimensional linear system via sampling the integral at nodes on each triangle, which we will denote by \mathbf{x}_{ij} , $j = 1, \dots, n_p$, and associating with each of these nodes a quadrature weight w_{ij} . The linear system is then enforced at each of the discretization nodes, resulting in the set of equations:

$$\sigma(\mathbf{x}_{ij}) + \sum_{k,l} w_{kl} R(\mathbf{x}_{ij}, \mathbf{x}_{kl}) \sigma(\mathbf{x}_{kl}) \sqrt{\det g(\mathbf{x}_{kl})} = f(\mathbf{x}_{ij}), \quad (6.3)$$

for $i = 1, \dots, M$ and $j = 1, \dots, n_p$, and where $\mathbf{x}_{kl} = \mathbf{y}_k(u_l, v_l)$ is the image of the Vioreanu-Rokhlin [71] quadrature node (u_l, v_l) on the reference simplex T_0 . The order of the quadrature is denoted by p , and the resulting number of nodes on each triangle is given by $n_p = p(p+1)/2$. See [11, 35] for a thorough discussion of this type of discretization and quadrature rule. The overall size of the linear system is then given by $N = Mn_p$. We will abbreviate our approximation to the solution σ at the discretization nodes by $\sigma_{ij} \approx \sigma(\mathbf{x}_{ij})$.

In our modified Nyström method different quadrature rules are used depending on the distance from the image of a particular map \mathbf{x}_k to a particular *target* node \mathbf{x}_{ij} . These rules can be split into three categories, as described in [35]: (1) singular quadrature, (2) nearly singular quadrature, and (3) smooth quadrature. While not all of the kernels discussed in this paper are actually singular at the origin, their behavior near the origin differs sufficiently from their far field behavior that different quadrature rules should be used to obtain suitable accuracy and speed. We now discuss the quadrature schemes used for these three categories, as well as for *edge quadrature* for surfaces with boundaries, for the kernels of interest in this work.

6.1.1 Singular quadrature

For curvilinear patches of integration in the above integral equation that contain the target point, it is necessary to use a quadrature rule that can integrate irregular or singular functions to high-order accuracy. (We refer to this as singular quadrature, even though in some cases the kernel is actually bounded.) In order to design this quadrature rule, we make the following observation about the remainder kernel.

Theorem 25. Let $\mathbf{y} = \mathbf{y}(r, \theta)$ be a local parameterization of Γ containing the point \mathbf{x} , and let the coefficients a , \mathbf{b} in the underlying surface PDE be smooth. If (r, θ) are polar coordinates centered at the pre-image of \mathbf{x} , then we have the following asymptotic formula as $r \rightarrow 0$:

$$R(\mathbf{x}, \mathbf{y}(r, \theta)) = \frac{(\nabla_{\Gamma} a + \mathbf{b}) \cdot \nabla_{\Gamma} \mathbf{y}|_{(0,0)} \hat{\boldsymbol{\theta}}}{r} - \frac{H^2(\mathbf{x}) \sin^2(2(\theta - \theta_{\star})) + \kappa_G(\mathbf{x}) \cos^2(2(\theta - \theta_{\star}))}{4\pi} + \mathcal{O}(r) \quad (6.4)$$

where $\hat{\boldsymbol{\theta}}$ is the unit vector in the θ -direction in the uv -plane, θ_{\star} is the angle corresponding to first the principal direction, and κ_G is the Gaussian curvature.

Proof. The proof is the same as in the derivation of (3.18), except that we use the curve γ defined by $\mathbf{y}(\cdot, \theta)$ and the asymptotic formulas for the derivatives of G appearing in (4.25). \square

Based on this observation, it is possible to use polar coordinates in the uv -plane to integrate the remainder kernel over the triangle containing the target point. In these coordinates, the contribution to the integral becomes

$$\int_{\Gamma_i} R(\mathbf{x}, \mathbf{x}') \sigma(\mathbf{x}') da(\mathbf{x}') = \int_0^{2\pi} \int_0^{L(\theta)} R(\mathbf{y}(0, 0), \mathbf{y}(r, \theta)) \sigma(\mathbf{y}(r, \theta)) \sqrt{\det g(r, \theta)} r dr d\theta, \quad (6.5)$$

where $L(\theta)$ is the distance from the pre-image of the target point to the edge of T_0 along the ray at angle θ to the x -axis. Due to the asymptotic formula (6.4), this change of coordinates has removed the singularity from the integrand. We may therefore use a smooth quadrature rule for this integral.

To this end, we discretize the inner and outer integrals in (6.5) using Gauss-Legendre quadrature. The panels for the inner integral are chosen adaptively. Additional care must be taken for the outer integral in θ since the upper bound of the inner integral, $L(\theta)$, is only piecewise smooth and becomes nearly singular as the center of the polar coordinates approaches the edge of the triangle, see Figure 4. We therefore adaptively choose our panels to resolve this near singularity. Specifically, we choose panels such that $L^2(\theta)$ is integrated to a pre-specified tolerance; this choice corresponds to integrating a bounded function of r to within the same tolerance. Since $L(\theta)$ is bounded by $\sqrt{2}$, this refinement will also be sufficient to integrate the logarithmic singularity in the parametrix. An example of the quadrature nodes used is shown in Figure 5.

Remark 3. It is unfortunately the case that the quadrature nodes used to accurately compute the integrals above do not coincide with the Vioreanu-Rokhlin nodes used in the discretization of the integral equation. In this case, it is required that we implicitly interpolate the function σ to the quadrature grid using interpolation matrices described in [35]. Composing these interpolation operators with the quadrature described above yields the required matrix entries in the discretized system. An analogous procedure for integrals which are nearly singular is discussed in the following section, Section 6.1.2.

We conclude this section by testing the previously described singular quadrature routine. We test it on three different functions of the form $F(r, \theta) \sigma(x, y)$, where (r, θ) are polar coordinates centered at the target point \mathbf{x} . The function $F(r, \theta)$ is set to either $\cos(2\theta)$ or $\log r$, which have the same singularity as R and K respectively. The function σ was set to 1, $\exp(x + y)$, or $\cos(\pi x)$. For this test, we use 16th-order Gauss-Legendre quadrature panels and check the convergence of the method with the integration tolerance by comparing it to the value given by the same routine with a finer tolerance. To fully test the method, we set \mathbf{x} to each of the target points that will be used in the global solver, i.e. the 16th-order Vioreanu-Rokhlin nodes. The results in Figure 6a show that the integration routine converges at the expected rate, independent of the test function.

6.1.2 Nearly singular quadrature

While changing to polar coordinates allows for the accurate computation of integrals over a triangle containing the target point, it cannot be used for adjacent triangles, as, in general, the pre-image

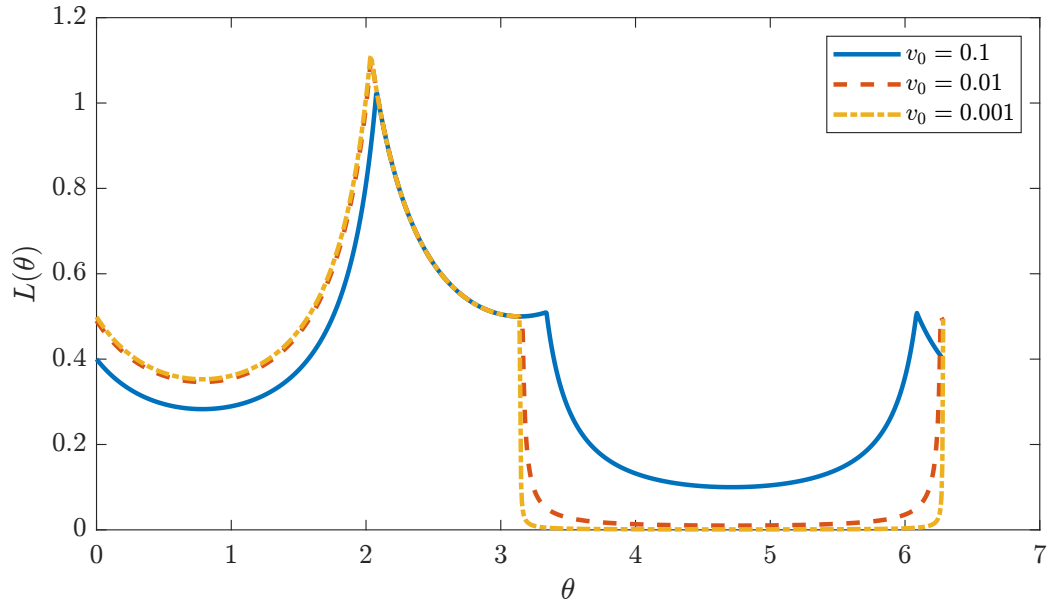


Figure 4: This figure shows an example of $L(\theta)$, where the polar coordinates are centered at $(0.5, v_0)$ for various choices of v_0 . For any center, $L(\theta)$ is a piecewise-smooth function, but as the center approaches the edge, it becomes nearly singular.

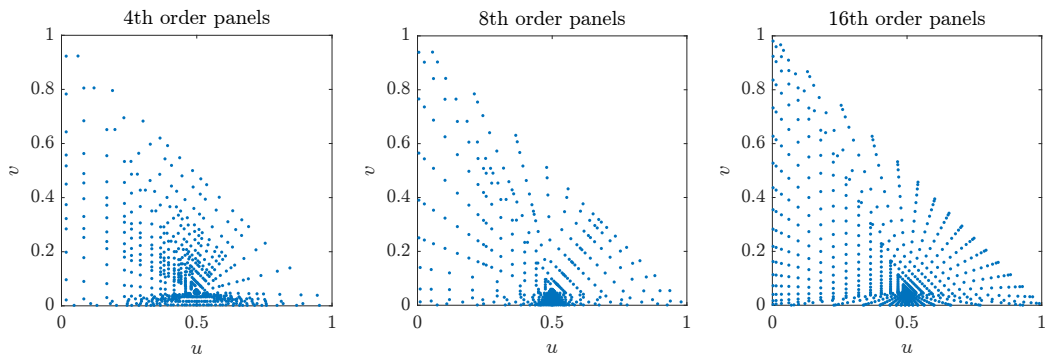
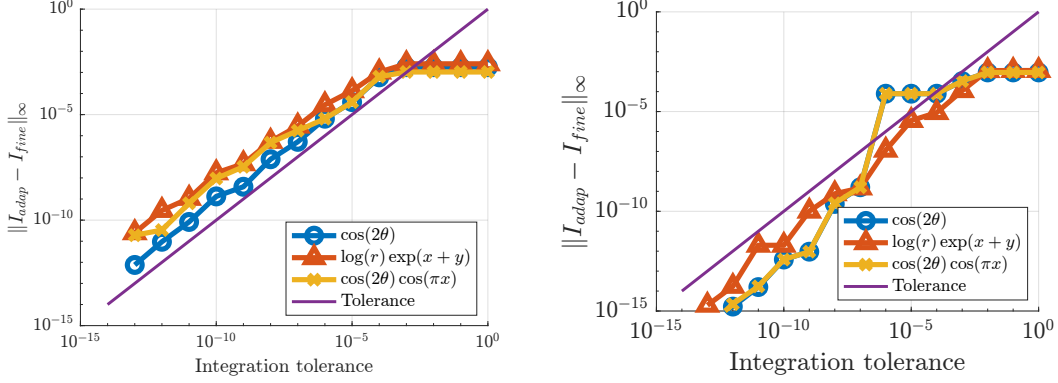


Figure 5: The polar tensor product grid used to compute the self contribution when the pre-image of the target is $(0.5, 0.05)$. For illustrative purposes, this grid is generated using 4th, 8th, and 16th order Gauss-Legendre panels. Our numerical examples will only use 16th order panels.



(a) The error in the singular quadrature routine when compared to the answer obtained using a finer tolerance. The solid line represents the error scaling with the integration tolerance.

(b) The error in the adaptive integrator when compared to the answer obtained using a finer tolerance. The solid line represents the error scaling with the integration tolerance.

Figure 6: The results of a convergence test for singular quadrature and adaptive integration routines applied to functions of the form $F(r, \theta)\sigma(x, y)$ for different choices of F and σ . Both tests involve repeating the experiment for a number of different target locations and reporting the maximum error observed over all test points. The figures demonstrates that both routines can be used to integrate functions with the (near-) singularities present in \mathcal{R} and \mathcal{K} to the desired tolerance.

of the target point in uv -plane is not known. For these nearly singular interactions, the adaptive integration method introduced in [11] and further developed in [35] can be used to compute the integrals to a specified accuracy. Before continuing, we define what we mean by a triangle *near* the target point. We first define the centroid of each triangle as the average position of its vertices. The radius of the triangle is then the largest distance from the centroid to a vertex. We shall then say that a target is near to a triangle if it is within 1.5 radii of the centroid of that triangle.

To compute the integral over triangles in the near field, we implicitly construct the polynomial interpolant $\tilde{\sigma}$ that agrees with the density $\sigma(\mathbf{y}_i(u, v))$ at the Vioreanu-Rohklin nodes. We shall write the interpolant in the basis of Koornwinder polynomials, a family of orthogonal polynomials on the simplex:

$$\tilde{\sigma}(u, v) = \sum_{n=1}^{n_p} c_n K_n(u, v). \quad (6.6)$$

One feature of the Vioreanu-Rohklin nodes is that the above polynomial interpolation is very well conditioned in this basis [71]. To find the coefficients, we define the matrix \mathbf{V} with coefficients

$$\mathbf{V}_{nj} = K_n(u_j, v_j). \quad (6.7)$$

The coefficients c_n may be then found via the formula:

$$c_n = \sum_{j=1}^{n_p} \mathbf{U}_{nj} \sigma(\mathbf{x}_i(u_j, v_j)), \quad (6.8)$$

where \mathbf{U}_{nj} is the nj -entry of the matrix $\mathbf{U} = \mathbf{V}^{-1}$. We can now compute the integral over the neighboring triangle as

$$\begin{aligned} \int_{\Gamma_i} R(\mathbf{x}, \mathbf{x}') \tilde{\sigma}(\mathbf{x}') da(\mathbf{x}') &= \sum_n c_n \int_T R(\mathbf{x}, \mathbf{y}(u, v)) K_n(u, v) \sqrt{\det g(u, v)} du dv \\ &= \sum_{n,j} \sigma(\mathbf{y}_i(u_j, v_j)) \mathbf{U}_{nj} \int_T R(\mathbf{x}, \mathbf{y}(u, v)) K_n(u, v) \sqrt{\det g(u, v)} du dv. \end{aligned} \quad (6.9)$$

The remaining integrals are independent of σ and may be precomputed to accelerate quadrature. In practice, they are computed by adaptively splitting T and using Vioreanu-Rohklin quadrature on each subtriangle [35].

We finish this section by testing our nearly singular quadrature routine. We test it on three different functions of the form $F(r, \theta)\sigma(x, y)$, where (r, θ) are polar coordinates centered at the target point \mathbf{x} outside the simplex and F and σ are chosen to be the same as in Section 6.1.1. For this test, we compare it to the value given by our routine using an oversample quadrature rule. To fully test the method, we set \mathbf{x} to each of the 16th-order Vioreanu-Rohklin nodes in a neighbouring triangle. The results in Figure 6b show that the error in our adaptive integration routine scales with our integration tolerance, independent of the test function.

6.1.3 Smooth quadrature

For integral contributions in (6.2) for which the target \mathbf{x} is sufficiently far from the domain of integration, i.e. not on Γ_i and not in the near field of Γ_i , the integrand can be treated as a smooth function and a quadrature rule for smooth functions can be applied. In particular, these portions of the integral equation are discretized using the Vioreanu-Rohklin quadrature rules for smooth functions on triangles [11, 71]. The resulting contributions to the finite dimensional linear system are purely Nyström in style:

$$\begin{aligned} \int_{\Gamma_i} R(\mathbf{x}, \mathbf{y}) \sigma(\mathbf{y}) da(\mathbf{y}) &= \int_{T_0} R(\mathbf{x}, \mathbf{y}_i(u, v)) \sigma(\mathbf{y}_i(u, v)) da(\mathbf{y}_i(u, v)) \\ &\approx \sum_{k,l} w_{kl} R(\mathbf{x}_{ij}, \mathbf{x}_{kl}) \sigma(\mathbf{x}_{kl}) \sqrt{\det g(\mathbf{x}_{kl})}. \end{aligned} \quad (6.10)$$

The quadrature nodes and weights are obtained from a precomputed lookup table based on the algorithm in [71].

6.1.4 Edge quadrature

For problems with boundaries, it is also necessary to construct a discretization of integrals along one-dimensional curves in \mathbb{R}^3 . We shall suppose that each boundary (curve) has a smooth and periodic parameterization, $\gamma : [0, 2\pi] \rightarrow \mathbb{R}^3$ with $\gamma(0) = \gamma(2\pi)$. The curve $\gamma = \gamma(t)$ is then sampled at equispaced points in t . Since we only consider boundaries that are smooth and closed curves, this allows for the use of spectrally accurate trapezoidal quadrature rules to compute smooth integrals.

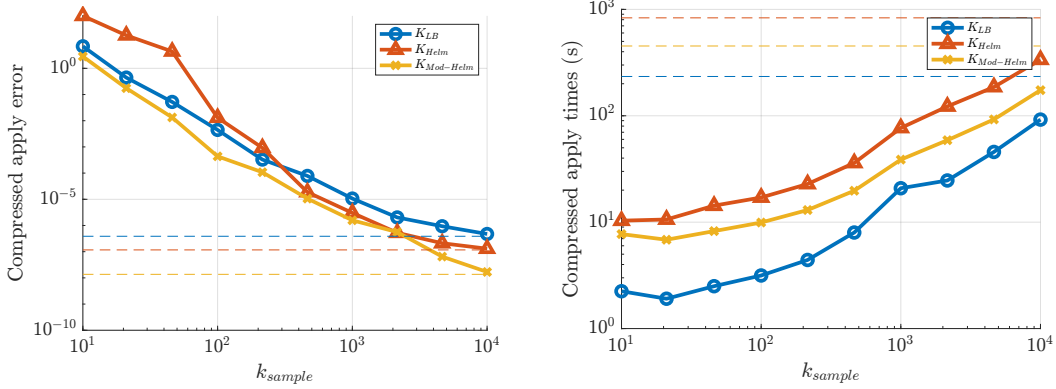
Computing the boundary-to-surface integral operators requires computing nearly singular integrals. For these integrals, the boundaries and densities supported on them are over-sampled by some fixed factor using Fourier interpolation; trapezoidal quadrature is then used on this over-sampled discretization. While this method is not spatially adaptive, it can still be used to solve a wide range of problems to high-order accuracy and is, more importantly, *not* a dominant cost of the discretization due to the one-dimensional nature of the boundary curve.

The performance of this discretization and quadrature scheme is discussed in Section 7.5.

6.2 Fast matrix vector multiplication

Coupling a fast matrix vector application with iterative Krylov methods, such as GMRES, generally results in accelerated solvers when the number of iterations required for convergence remains bounded and $\mathcal{O}(1)$. In order to efficiently apply the dense integral operators appearing in the parametric formulation of this paper, we use a modification of the *interpolative fast multipole method* (IFMM) [58]. As with all fast multipole methods (FMMs), this method is based on the observation that if a block of the kernel matrix corresponds to an interaction between well-separated sources and targets then it will be of low numerical rank due to the smoothness of the kernel function. The method then exploits this observation by organizing the discretization points \mathbf{x}_i into an octree and compressing the interaction of points in the blocks corresponding to the points in different boxes at the same level in the octree.

In standard fast multipole method fashion, the computational domain (in this case, discretization points on the surface Γ) is hierarchically partitioned via an octree. Denoting the boxes in the octree



(a) The error induced in the N -body calculation (6.13) when the IFMM tolerance is set to 10^{-9} and k_s is varied. The dashed line represents the error in the IFMM without randomized compression.

(b) The total time to use our IFMM to compute the N -body calculation (6.13) as a function of k_s . The dashed line represents the time to use the IFMM without randomized compression.

Figure 7: The results of increasing k_s in our IFMM. We see that for $k_s = 10,000$, the IFMM has the same accuracy as the deterministic IFMM, but only involves a 17% of the points. This fact allows us to compute the IFMM to the same tolerance in a fraction of the time.

as B_k and indices of the nodes/points in box B_k by l_k , then the IFMM approximates the interaction between B_k and B_l by

$$\sum_{j \in l_k} K(\mathbf{x}, \mathbf{x}_j) a_j \approx \sum_{j \in J_{kl} \subset l_k} K(\mathbf{x}, \mathbf{x}_j) b_{jl}, \quad \text{for all } \mathbf{x} \in B_l, \quad (6.11)$$

where J_{kl} is a specially chosen subset of l_k and the new coefficients/weights b_{kl} are computed based on the a_j 's and the choice of J_{kl} . This approximation is computed using an interpolative decomposition. We recall that an exact interpolative decomposition of a matrix is given by the following definition:

Definition 4. Let \mathbf{A} be an $m \times n$ matrix with rank k . An interpolative decomposition (ID) of \mathbf{A} is a factorization of the form

$$\mathbf{A} = \mathbf{A}(:, \mathbf{J}) \mathbf{X}, \quad (6.12)$$

where \mathbf{X} is a $k \times n$ matrix and \mathbf{J} is a set of k indices between 1 and n .

In practice, interpolative decompositions are computed so that the above factorization is accurate (in a relative sense) to some user-specified precision $\epsilon > 0$. These ϵ -accurate IDs can be computed numerically, for example, using a rank-revealing column-pivoted QR decomposition, and described in [56]. The ID is closely related to the idea of skeletonization, and \mathbf{J} in the definition above is referred to as the skeleton of the matrix \mathbf{A} .

The required skeletons J_{kl} in (6.11) can be computed by finding an approximate ID of the matrix

$$\mathbf{K}^{lk} = [K(\mathbf{x}_i, \mathbf{x}_j)]$$

for $i \in l_l$ and $j \in l_k$. In practice however, this cost is prohibitively expensive because the sizes of the largest blocks scale with the number of unknowns. Instead, most implementations make use of a so-called *proxy surface* [57, 75]. Typically, this involves prescribing a number of test points $\tilde{\mathbf{x}}_i$ which lie on a sphere P_{kl} containing B_k but not B_l . The skeleton is then found by computing the ID of the much smaller matrix $[K(\tilde{\mathbf{x}}_i, \mathbf{x}_j)]$ with $i \in P_{kl}$ and $j \in l_k$. This approach is justified by using Green's identities for elliptic PDEs in \mathbb{R}^3 [35] and is therefore only applicable if the kernel is some combination of derivatives of a three-dimension Green's function.

Since the kernels appearing in the integral equations of this work are *not* formally PDE-kernels, as an alternative method to accelerate the compression we compute an ID of the matrix \mathbf{K}^{lk} by picking k_s target points (i.e. rows) from \mathcal{I}_l and k_s source points (i.e. columns) from \mathcal{I}_k . This class of methods has been previously explored in [74]. In this paper, we use the simplest version of this

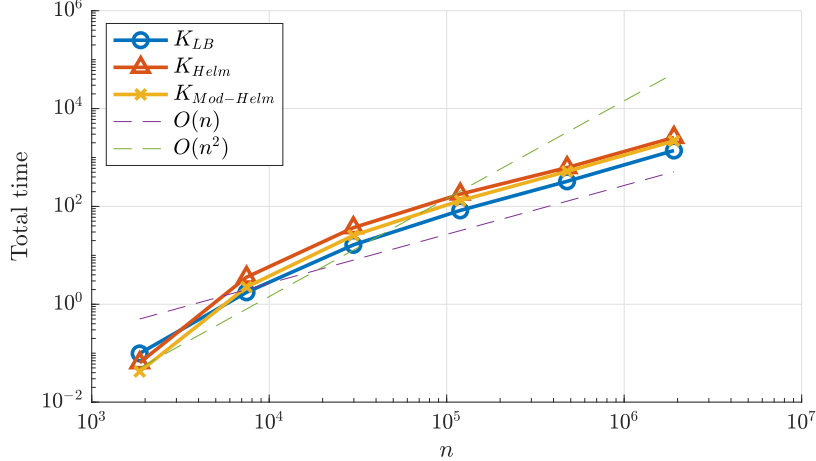


Figure 8: The time to build and apply our IFMM on successively finer discretizations of a wavy torus.

algorithm where the sampled points are chosen randomly. In order for this sampling to be robust, the random subset should be chosen to cover the both B_k and B_l . In practice, however, we have found that choosing points independent of target and source locations has proved effective in the numerical examples presented below. Our particular implementation is based on the implementation of the IFMM found in the FLAM package [41].

The approximation accuracy of our implementation of the IFMM is validated by comparing it to the direct matrix apply. We perform an N -body calculation

$$\varphi_i = \sum_{j \neq i} F(\mathbf{x}_i, \mathbf{x}_j) \sigma_j, \quad (6.13)$$

where the \mathbf{x}_i 's are a discretization of a wavy torus shown in Figure 10 using 58,752 points. (The same geometry is used later on in the numerical experiments section.) We choose $\sigma_i = (\mathbf{x}_i)_1 + \eta_i$ where $(\mathbf{x}_i)_1$ denotes the x -coordinate of \mathbf{x}_i and η_i is a realization of a standard normal random variable. In Figure 7a we show the l^2 error between the direct calculation and the IFMM result, and how that error depends on the choice of k_s . In Figure 7b we show how our randomized compression accelerates the IFMM. In all of these tests, we set the relative ID compression tolerance to 10^{-9} . We provide three different cases in each subplot in Figure 7: (1) with F set to the parametrix for the Laplace-Beltrami problem, (2) F set to the parametrix for the Helmholtz-Beltrami problem, and (3) with F set to the modified-Helmholtz-Beltrami parametrix. We also tested with F set to the associated remainder functions and found similar results.

Lastly, we also test the complexity of this scheme using the same surface and numerical tolerance as in the previous test; k_s is set to 10,000. The time taken to build and apply with various different surface discretizations is shown in Figure 8. Once $N > k_s$, we see that the method scales as $O(N)$.

7 Numerical Experiments

In this section, we report the results of some numerical examples demonstrating the integral equation solvers detailed above. In all of the tests, GMRES was used to solve the linear system. The GMRES, integration, and compression tolerances were set to 10^{-9} . In all tests, our errors are measured in the relative L^2 sense. In all tests we set $k_s = 10,000$ because the above experiments indicate that that is enough samples for the IFMM to achieve the same error as the deterministic method with this tolerance.

We shall conduct tests on three surfaces: the unit sphere (Figure 9a); an ellipsoid with semi axis lengths 4.5, 2.25, and 3 (Figure 10, left); and a wavy torus (Figure 10, right), given by the

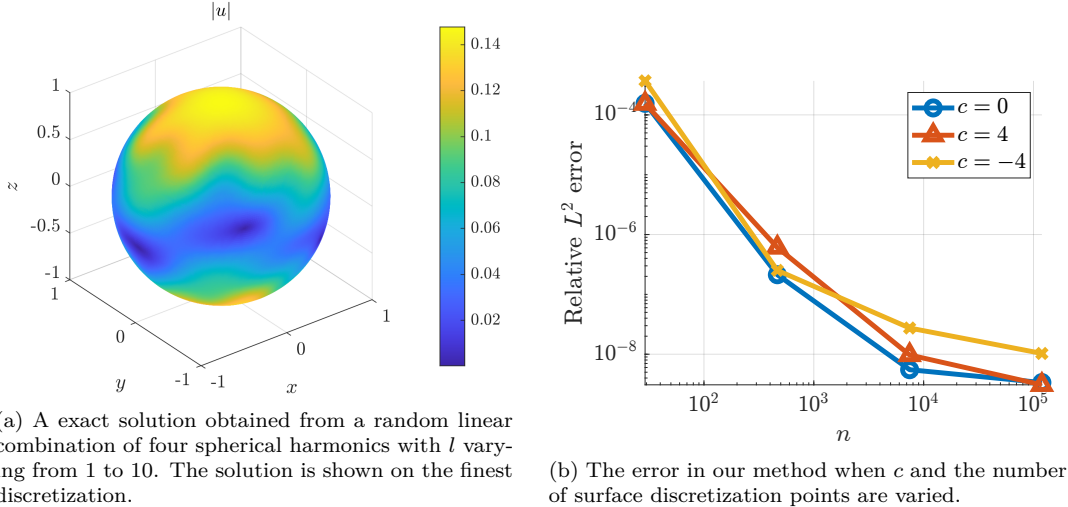


Figure 9: The results of testing our parametrized solver on a sphere.

parameterization

$$\mathbf{r}(u, v) = \begin{bmatrix} (3 + \cos(v) + 0.6 \cos(5u)) \cos(u) \\ (3 + \cos(v) + 0.6 \cos(5u)) \sin(u) \\ \sin(v) \end{bmatrix} \quad \text{where } (u, v) \in [0, 2\pi)^2. \quad (7.1)$$

In Section 7.5, where we solve boundary value problems, we consider Γ to be the wavy torus with u restricted to lie in $(4\pi/3, 2\pi)$.

7.1 Spherical harmonic validation

It is well known that the spherical harmonics Y_l^m are the eigenfunctions of the Laplace-Beltrami operator on a sphere; their eigenvalues are $-l(l+1)$. Since the spherical harmonics form an orthogonal basis for L^2 on the sphere, we can expand any f in terms of the spherical harmonics by computing inner products. We can then analytically solve of the Laplace-Beltrami problem by dividing the expansion coefficients by the corresponding eigenvalues and then summing the resulting expansion.

We used this observation to test our method by letting f be a random linear combination of Y_1^0, Y_3^3, Y_{10}^6 , and Y_{10}^7 and comparing the solution given by our solver to the analytic solution (Figure 9a). Since adding a constant c to the Laplace-Beltrami operator simply adds c to the eigenvalues, we can use the same method to test our solver for the Helmholtz- and modified Helmholtz-Beltrami problems. The errors in our computations are shown in Figure 9b. We can see that the method converges to around the specified tolerance for each value of c . The solver had slightly less accuracy when c was negative because the singular quadrature routine was not designed for the exponential decay in the parametrized.

7.2 A Laplace-Beltrami problem

In order to validate our Laplace-Beltrami solver on a broader class of surfaces, we use the method of manufactured solutions. Following the approach in [62], we did this by choosing Γ to be a smooth surface and choosing the exact solution to be a constant plus the restriction of a smooth function v defined in all of \mathbb{R}^3 . We then generated the corresponding right hand side f by applying the formula (4.27) to v :

$$f = \Delta_\Gamma (v|_\Gamma) = \Delta v - 2H \frac{\partial v}{\partial \mathbf{n}} - \frac{\partial^2 v}{\partial \mathbf{n}^2}. \quad (7.2)$$

We evaluate f by analytically computing the terms in (7.2) based on a global parameterization of the surface.

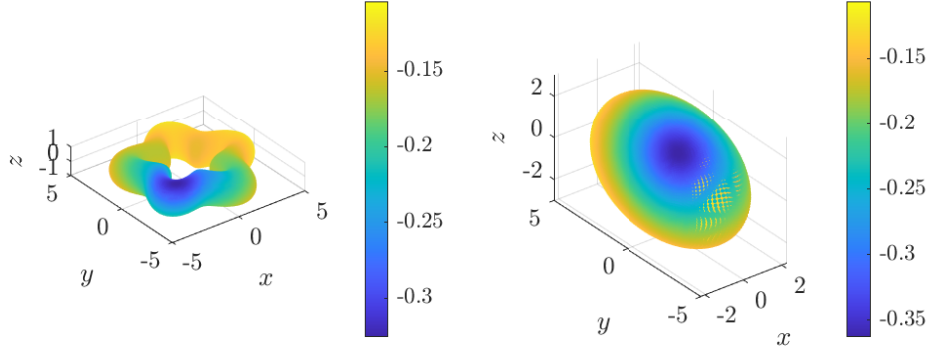


Figure 10: The reference solution for the Laplace-Beltrami solver on two choices of Γ .

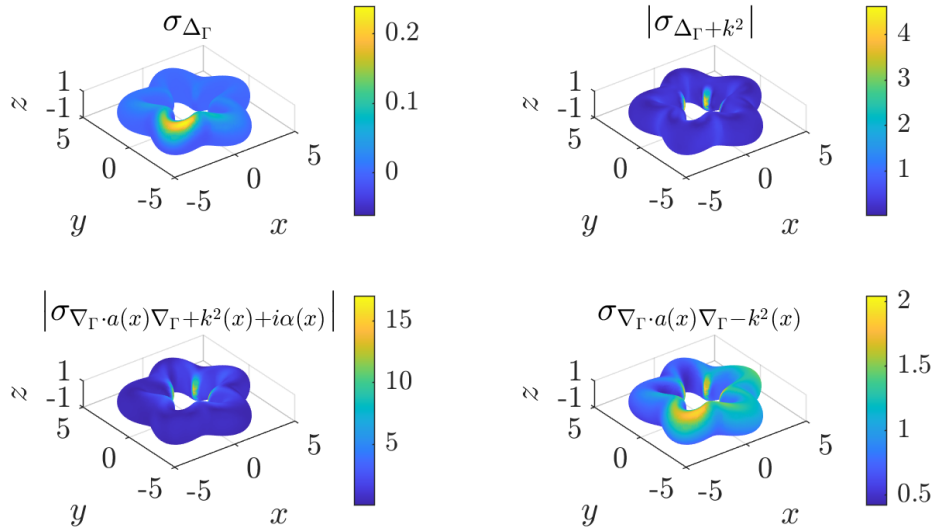


Figure 11: The solution densities on a wavy torus for various surface PDEs. All densities correspond to the same solution u .

In this example, Γ is given by either a wavy torus or an ellipsoid (Figure 10). We set v to be the Newtonian potential centered at $\mathbf{x}_0 = (-3, -3, 4)$, which is a point outside of, but fairly close to, both choices for Γ :

$$v(\mathbf{x}) = -\frac{1}{|\mathbf{x} - \mathbf{x}_0|}.$$

The exact solution to this problem is given by $u = v|_{\Gamma} - \frac{1}{|\Gamma|} \int_{\Gamma} v$, where $|\Gamma|$ is the surface area of Γ . The reference solutions are shown in Figure 10. We conducted a convergence test by repeatedly refining the triangles used in our surface discretization and thus varying n . We can see from Figures 13a and 14a that our method is capable of achieving small relative errors, and therefore the solver is working as expected. From Figures 13b and 14b, we can see that the computational time of our method increases super-linearly, but not quadratically on the tested range, so our fast apply is working and our matrices are indeed compressible.

7.3 A Helmholtz-Beltrami problem

We now test our method on the Helmholtz-Beltrami problem with c set to the moderate value of 4. As before, we use the method of manufactured solutions. We again let v be a Newtonian potential and we set the solution to be $u = v|_{\Gamma}$ and construct the right hand side $f = \Delta_{\Gamma}(v|_{\Gamma}) + cv|_{\Gamma}$, where

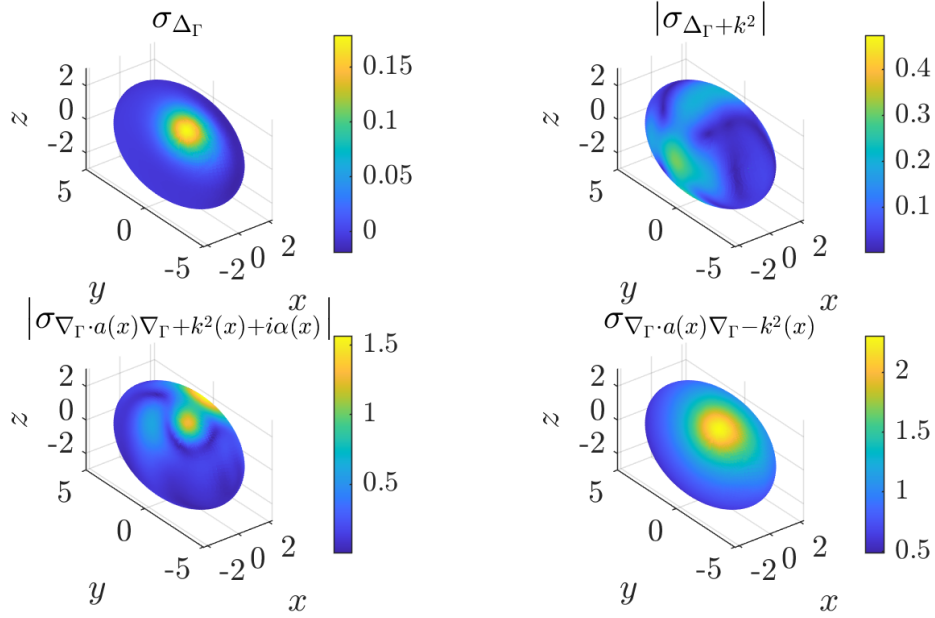
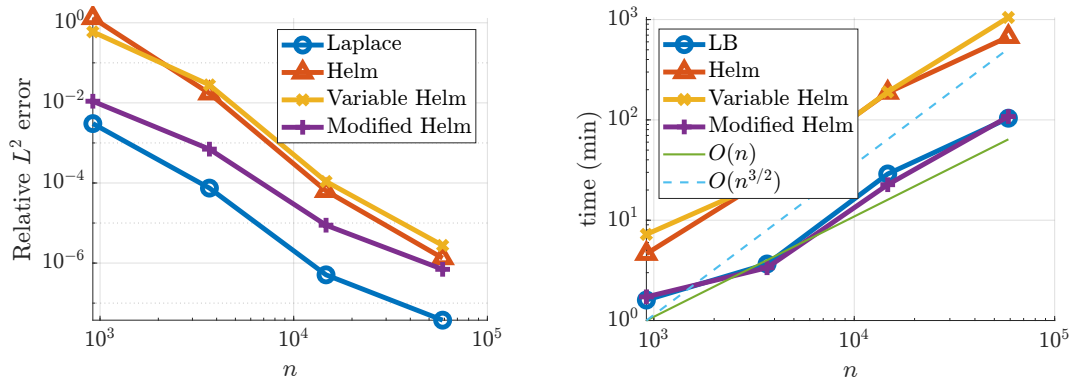


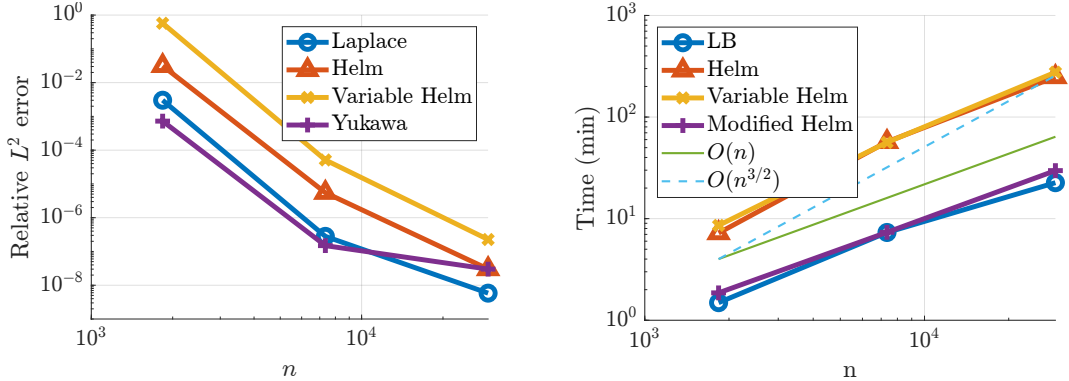
Figure 12: The solution densities on an ellipsoid for various surface PDEs. All densities correspond to the same solution u



(a) The errors of the computed solution in the wavy torus tests where n is the number of points used to discretize the surface.

(b) The time to compute the solution in the wavy torus tests where n is the number of points used to discretize the surface.

Figure 13: Results of the wavy torus tests.



(a) The errors of the computed solution in the ellipsoid tests where n is the number of points used to discretize the surface.

(b) The time to compute the solution in the ellipsoid tests where n is the number of points used to discretize the surface.

Figure 14: Results of the ellipsoid tests.

we have again used (4.27) to compute f analytically. The results of our tests are shown in Figures 13 and 14. We see that the method is less accurate on this surface PDE, but still converges at a similar rate. In Figures 11 and 12, we see that this limited accuracy is likely due to the fact that the density σ is not sufficiently resolved. Figure 13 also shows that the solver takes longer to solve the Helmholtz-Beltrami problem than the Laplace-Beltrami problem. This was predominantly caused by the increased number of GMRES iterations required to solve the linear system.

7.4 A variable coefficient surface PDE

In this experiment, we test our method on a problem where the parameters a and c are not constant. In this case, the remainder kernel R is weakly singular, but adaptive integration can still be used to accurately discretize the integral equation. We use the same singular quadrature routine as before due to the fact that the singularity in R will be cancelled via the change to polar coordinates. We test our code in the same way as before, by choosing $u = v|_{\Gamma}$, where v is a Newtonian potential and analytically computing the corresponding right hand side.

For this experiment, we set a to be a linear function of the coordinate z , chosen to vary by a factor of three over the surface. We also set $c = -4 - \exp(x/2)$. We also tested our solver with $a = 1 + \exp(z)$ and $c = 4(1 + 0.2y + 0.2i \sin x)$.

We can see from Figures 13 and 14 that introducing variable coefficients did not greatly impact the error in the solution or the time to compute it.

7.5 Boundary value problems

We now test our method for solving the Laplace-Beltrami equation with Neumann or Dirichlet boundary conditions. We choose Γ to be a subset of the wavy torus from the previous three sections. The performance of this discretization is tested by estimating the error in applying the operators \mathcal{R}_γ and \mathcal{T}_γ to a specified function μ on the example surface shown in Figure 15. As before, we set all of our IFMM tolerances to 10^{-9} . We construct a discretization of the surface using the method above, and sample each boundary (curve) using 200 points equispaced in the parameterization variable. We estimate the quadrature error by comparing to the values given by the finest discretizations. In this test we chose $\mu = \exp(x)$ and used the operators \mathcal{R}_γ and \mathcal{T}_γ as in the Laplace-Beltrami problem. The estimated errors for various oversampling factors are shown in Figure 16. We can see that once the near singularity is resolved, the error decays quite quickly. We can also see that more points are required to resolve the singularity when the surface discretization is refined and discretization nodes are brought closer to the boundary.

We now test our solver for surface boundary value problems. We again choose the solution u to be

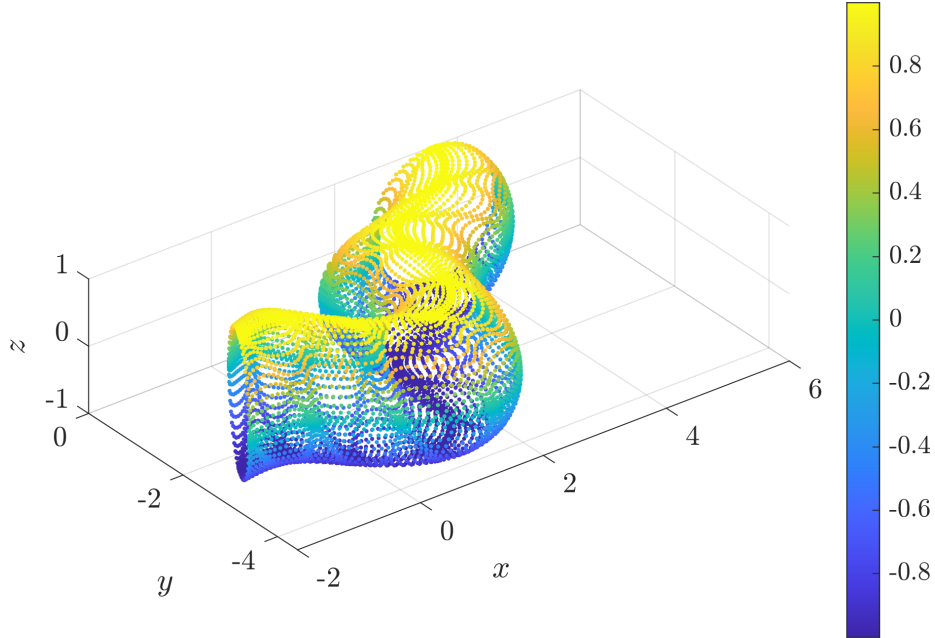


Figure 15: The example surface for the edge quadrature test.

the restriction of a Newtonian potential to Γ and analytically compute the corresponding f and f_γ . Each subset of $\gamma = \partial\Gamma$ is discretized with n_φ equispaced nodes and we set the oversampling factor to 64. In subsequent tests, we refined our discretization by independently splitting each triangle in our surface discretization and doubling the number of points used to discretize each boundary.

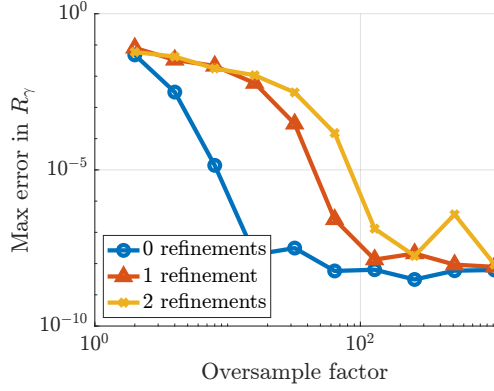
The results of our tests are shown in Figure 17. We can see that as both the surface and edge discretizations are refined, the error decreases as expected. As in the edge quadrature test, the stronger singularity in the kernel \mathcal{T}_γ results in the Dirichlet boundary value problem requiring an increased number of points in order to achieve a similar accuracy.

8 Conclusion

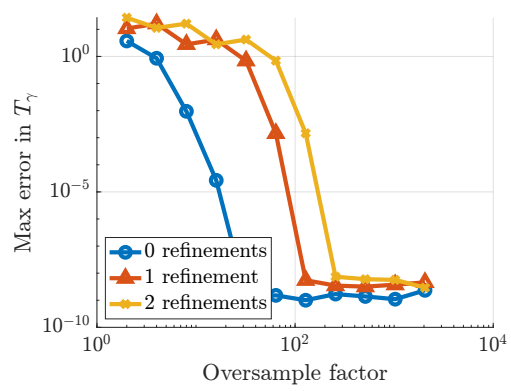
In this work we have presented a general framework for reformulating variable coefficient surface PDEs as boundary integral equations using a family of parametrices that scale according to the coefficients in the particular surface PDE in question. The resulting integral equations are second-kind and quite well-conditioned. Furthermore, we've demonstrated via a battery of numerical examples that they can be rapidly solved using a combination of hierarchical linear algebraic compression coupled with an iterative solver, such as GMRES. The associated kernels of the integral equations are either bounded or weakly singular, and some special-purpose quadrature schemes were developed to accurately compute the boundary integrals.

Going forward, the analytical and numerical ideas presented here can be extended in various ways, including to solving problems on curves in two dimensions and for solving anisotropic problems, i.e., problems with leading term $\nabla_\Gamma \cdot \mathbf{A} \nabla_\Gamma$, where \mathbf{A} is non-degenerate (possibly non-constant) matrix. In this latter case, preliminary choices for a parametrix resulted in integral equations having kernels which were quite singular. Additional analysis and numerical experiments are required to develop a more suitable parametrix.

Lastly, there is significant evidence that even faster matrix-vector multiplies can be obtained using a more careful analysis of the remainder kernels, in the style of multipole expansions for true PDE kernels (such as $1/r$ or e^{ikr}/r). Developing such fast algorithms is actively being investigated.

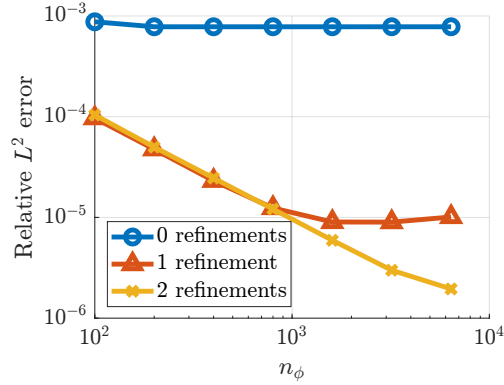


(a) The test with \mathcal{R}_γ , which is required for the Neumann boundary value problems.

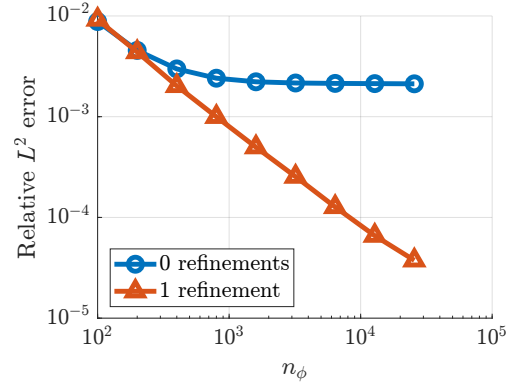


(b) The test with \mathcal{T}_γ , which is required for the Dirichlet boundary value problems.

Figure 16: This graph shows how the error in the application of \mathcal{R}_γ and \mathcal{T}_γ depends on the oversampling factor and the density of the surface discretization.



(a) The error in the Neumann boundary value solver.



(b) The error in the Dirichlet boundary value solver.

Figure 17: The error in our boundary value problem solvers. In these tests we measure the L^2 error as we refine the surface and edge discretizations.

References

- [1] D. Agarwal, M. O’Neil, and M. Rachh. FMM-accelerated solvers for the Laplace-Beltrami problem on complex surfaces in three dimensions. *J. Sci. Comput.*, 97:25, 2023.
- [2] C. J. Alves and P. R. Antunes. The method of fundamental solutions applied to boundary value problems on the surface of a sphere. *Comp. Math. Appl.*, 75(7):2365–2373, 2018.
- [3] M. Andreux, E. Rodolà, M. Aubry, and D. Cremers. Anisotropic Laplace-Beltrami Operators for Shape Analysis. In L. Agapito, M. M. Bronstein, and C. Rother, editors, *Computer Vision - ECCV 2014 Workshops*, pages 299–312, Cham, 2015. Springer International Publishing.
- [4] S. Angenent, S. Haker, A. Tannenbaum, and R. Kikinis. On the Laplace-Beltrami Operator and Brain Surface Flattening. *IEEE Trans. Med. Imag.*, 18(8):700–711, 1999.
- [5] E. Bänsch, P. Morin, and R. H. Nochetto. A finite element method for surface diffusion: The parametric case. *J. Comput. Phys.*, 203(1):321–343, 2005.
- [6] L. Beirão da Veiga, F. Brezzi, L. D. Marini, and A. Russo. The hitchhiker’s guide to the virtual element method. *Math. Models and Meth. Appl. Sci.*, 24(08):1541–1573, 2014.
- [7] M. Bertalmío, L.-T. Cheng, S. Osher, and G. Sapiro. Variational problems and partial differential equations on implicit surfaces. *J. Comput. Phys.*, 174(2):759–780, 2001.
- [8] A. Beshley, R. Chapko, and B. T. Johansson. An integral equation method for the numerical solution of a Dirichlet problem for second-order elliptic equations with variable coefficients. *J. Eng. Math.*, 112(1):63–73, 2018.
- [9] A. Bonito, A. Demlow, and R. H. Nochetto. *Finite element methods for the Laplace-Beltrami operator*, volume 21. Elsevier B.V., 1 edition, 2020.
- [10] A. Bonito, A. Demlow, and J. Owen. A Priori Error Estimates for Finite Element Approximations to Eigenvalues and Eigenfunctions of the Laplace-Beltrami Operator. *SIAM J. Num. Anal.*, 56(5):2963–2988, 2018.
- [11] J. Bremer and Z. Gimbutas. A Nyström method for weakly singular integral operators on surfaces. *J. Comput. Phys.*, 231:4885–4903, 2012.
- [12] H. Brezis. *Functional analysis, Sobolev spaces and partial differential equations*. Universitext. Springer, New York
- [13] E. Burman, P. Hansbo, M. G. Larson, and A. Massing. A cut discontinuous Galerkin method for the Laplace-Beltrami operator. *IMA J. Num. Anal.*, 37(1):138–169, 2017.
- [14] E. Burman, P. Hansbo, M. G. Larson, and A. Massing. A stable cut finite element method for partial differential equations on surfaces: The Helmholtz-Beltrami operator. *Comput. Meth. Appl. Mech. Eng.*, 362:112803, 2020.
- [15] Y. Chen and C. B. Macdonald. The closest point method and multigrid solvers for elliptic equations on surfaces. *SIAM J. Sci. Comput.*, 37(1):A134–A155, 2015.
- [16] O. Chkadia, S. E. Mikhailov, and D. Natroshvil. Analysis of direct boundary-domain integral equations for a mixed BVP with variable coefficient, I: Equivalence and invertibility. *J. Integral Equ. Appl.*, 21(4):499–543, 2009.
- [17] O. Chkadia, S. E. Mikhailov, and D. Natroshvili. Analysis of direct boundary-domain integral equations for a mixed BVP with variable coefficient, II: Solution regularity and asymptotics. *J. Integral Equ. Appl.*, 22(1):19–37, 2010.

- [18] O. Chkadua, S. E. Mikhailov, and D. Natroshvili. Localized Boundary-Domain Singular Integral Equations Based on Harmonic Parametrix for Divergence-Form Elliptic PDEs with Variable Matrix Coefficients. *Integral Equ. Oper. Theory*, 76(4):509–547, 2013.
- [19] O. Chkadua, S. E. Mikhailov, and D. Natroshvili. Singular localised boundary-domain integral equations of acoustic scattering by inhomogeneous anisotropic obstacle. *Math. Meth. Appl. Sci.*, 41(17):8033–8058, 2018.
- [20] M. Chung and J. Taylor. Diffusion smoothing on brain surface via finite element method. In *2004 2nd IEEE International Symposium on Biomedical Imaging: Nano to Macro (IEEE Cat No. 04EX821)*, pages 432–435 Vol. 1, 2004.
- [21] A. Demlow and G. Dziuk. An adaptive finite element method for the Laplace–Beltrami operator on implicitly defined surfaces. *SIAM J. Num. Anal.*, 45(1):421–442, 2007.
- [22] G. Dziuk. Finite elements for the Beltrami operator on arbitrary surfaces. In *Partial differential equations and calculus of variations*, pages 142–155. Springer, Berlin, Heidelberg, 1988.
- [23] G. Dziuk and C. M. Elliott. Finite element methods for surface PDEs. *Acta Numer.*, 22:289–396, 2013.
- [24] C. L. Epstein and L. Greengard. Debye sources and the numerical solution of the time harmonic Maxwell equations. *Comm. Pure Appl. Math.*, dec 2009.
- [25] C. L. Epstein, L. Greengard, and M. O’Neil. Debye Sources and the Numerical Solution of the Time Harmonic Maxwell Equations II. *Comm. Pure Appl. Math.*, 66(5):753–789, 2013.
- [26] C. L. Epstein, L. Greengard, and M. O’Neil. A high-order wideband direct solver for electromagnetic scattering from bodies of revolution. *J. Comput. Phys.*, 387:205–229, 2019.
- [27] J. Escher, U. F. Mayer, and G. Simonett. The surface diffusion flow for immersed hypersurfaces. *SIAM J. Math. Anal.*, 29(6):1419–1433, 1998.
- [28] L. C. Evans. *Partial Differential Equations*. American Mathematical Society, Providence, Rhode Island, 2nd edition, 2010.
- [29] G. B. Folland. *Introduction to Partial Differential Equations*. Princeton University Press, Princeton, New Jersey, 2nd edition, 1995.
- [30] D. Fortunato. A high-order fast direct solver for surface PDEs. *SIAM J. Sci. Comput.*, 2023.
- [31] C. Fresneda-Portillo and Z. Woldemicheal. A new family of boundary-domain integral equations for the Dirichlet problem of the diffusion equation in inhomogeneous media with $H^{-1}(\Omega)$ source term on Lipschitz domains. *Math. Meth. Appl. Sci.*, 44(12):9817–9830, 2021.
- [32] C. Fresneda-Portillo and Z. W. Woldemicheal. On the existence of solution of the boundary-domain integral equation system derived from the 2D Dirichlet problem for the diffusion equation with variable coefficient using a novel parametrix. *Complex Var. Elliptic Equ.*, 65(12):2056–2070, 2020.
- [33] M. Frittelli and I. Sgura. Virtual element method for the Laplace-Beltrami equation on surfaces. *ESAIM: Math. Modell. Num. Anal.*, 52(3):965–993, 2018.
- [34] P. Garabedian. *Partial Differential Equations*. Chelsea Publish Company, New York, NY, 2nd edition, 1986.
- [35] L. Greengard, M. O’Neil, M. Rachh, and F. Vico. Fast multipole methods for the evaluation of layer potentials with locally-corrected quadratures. *J. Comput. Phys.: X*, 10:100092, 2021.
- [36] L. Greengard and V. Rokhlin. A fast algorithm for particle simulations. *J. Comput. Phys.*, 73(2):325–348, 1987.

- [37] P. Grinfeld. Hamiltonian Dynamic Equations for Fluid Films. *Studies in Applied Mathematics*, 125(3):223–264, 2010.
- [38] P. Grinfeld. Small oscillations of a soap bubble. *Stud. Appl. Math.*, 128(1):30–39, 2012.
- [39] J. Hadamard. Le problème de cauchy et les équations aux dérivées partielles linéaires hyperboliques. *Paris*, 11:243–264, 1932.
- [40] E. Hebey. *Nonlinear analysis on manifolds : Sobolev spaces and inequalities*, volume 5 of *Courant Lecture Notes in Mathematics*. American Mathematical Society, New York, NY, 2000.
- [41] K. Ho. FLAM: Fast Linear Algebra in MATLAB - Algorithms for Hierarchical Matrices. *J. Open Source Softw.*, 5(51):1906, 2020.
- [42] L. Hormander. *The Analysis of Linear Partial Differential Operators III*. Springer-Verlag, 1994.
- [43] G. C. Hsiao and W. L. Wendland. *Boundary integral equations*. Applied mathematical sciences (Springer-Verlag New York Inc.) ; v. 164. Springer, 2nd edition, 2021.
- [44] L. M. Imbert-Gérard and L. Greengard. Pseudo-Spectral Methods for the Laplace-Beltrami Equation and the Hodge Decomposition on Surfaces of Genus One. *Numerical Methods for Partial Differential Equations*, 33(3):941–955, 2017.
- [45] F. John. *Partial Differential Equations*. Springer-Verlag, New York, NY, 4th edition, 1982.
- [46] N. King, H. Su, M. Aanjaneya, S. Ruuth, and C. Batty. A closest point method for surface pdes with interior boundary conditions for geometry processing. *arXiv:2305.04711*, 2023.
- [47] J. Kromer and D. Bothe. Highly accurate numerical computation of implicitly defined volumes using the Laplace-Beltrami operator. *arXiv:1805.03136*, pages 1–25, 2018.
- [48] M. C. Kropinski and N. Nigam. Fast integral equation methods for the Laplace-Beltrami equation on the sphere. *Adv. Comput. Math.*, 40(2):577–596, 2014.
- [49] M. C. Kropinski, N. Nigam, and B. Quaife. Integral equation methods for the Yukawa-Beltrami equation on the sphere. *Adv. Comput. Math.*, 42(2):469–488, 2016.
- [50] K. A. Kuo and H. E. Hunt. The vibrations of bubbles and balloons. *Acoustics Australia*, 40(3):183–187, 2012.
- [51] P. D. Lax. *Functional analysis*, volume 55. John Wiley & Sons, 2002.
- [52] G. Leoni. *A First Course in Sobolev Spaces: Second Edition*. American Mathematical Society, Providence, Rhode Island, second edition, 2017.
- [53] C. B. Macdonald and S. J. Ruuth. Level set equations on surfaces via the closest point method. *J. Sci. Comput.*, 35:219–240, 2008.
- [54] C. B. Macdonald and S. J. Ruuth. The implicit closest point method for the numerical solution of partial differential equations on surfaces. *SIAM Journal on Scientific Computing*, 31(6):4330–4350, 2010.
- [55] D. Malhotra, A. Cerfon, L.-M. Imbert-Gérard, and M. O’Neil. Taylor States in Stellarators: A Fast High-order Boundary Integral Solver. *J. Comput. Phys.*, Feb 2019.
- [56] P.-G. Martinsson. *Fast direct solvers for elliptic PDEs*. SIAM, 2019.
- [57] P.-G. Martinsson and V. Rokhlin. A fast direct solver for boundary integral equations in two dimensions. *J. Comput. Phys.*, 205(1):1–23, 2005.
- [58] P.-G. Martinsson and V. Rokhlin. An accelerated kernel-independent fast multipole method in one dimension. *SIAM J. Sci. Comput.*, 29(3):1160–1178, 2007.

- [59] A. Naumovets and Y. S. Vedula. Surface diffusion of adsorbates. *Surface Science Reports*, 4(7-8):365–434, 1985.
- [60] J.-C. Nedélec. *Acoustic and Electromagnetic Equations*. Springer-Verlag, New York, NY, 2001.
- [61] I. L. Novak, F. Gao, Y.-S. Choi, D. Resasco, J. C. Schaff, and B. M. Slepchenko. Diffusion on a curved surface coupled to diffusion in the volume: Application to cell biology. *J. Comput. Phys.*, 226(2):1271–1290, 2007.
- [62] M. O’Neil. Second-kind integral equations for the Laplace-Beltrami problem on surfaces in three dimensions. *Adv. Comput. Math.*, 44(5):1385–1409, 2018.
- [63] M. O’Neil and A. J. Cerfon. An integral equation-based numerical solver for Taylor states in toroidal geometries. *J. Comput. Phys.*, 359:263–282, 2018.
- [64] J. Pouchin. Weakly singular integral operators as mappings between function spaces. *The Journal of Integral Equations and Applications*, pages 303–320, 1988.
- [65] M. Rachh. *Integral equation methods for problems in electrostatics, elastostatics and viscous flow*. PhD thesis, New York University, 2015.
- [66] A. Rahimian, I. Lashuk, S. Veerapaneni, A. Chandramowliswaran, D. Malhotra, L. Moon, R. Sampath, A. Shringarpure, J. Vetter, R. Vuduc, et al. Petascale direct numerical simulation of blood flow on 200k cores and heterogeneous architectures. In *SC’10: Proceedings of the 2010 ACM/IEEE International Conference for High Performance Computing, Networking, Storage and Analysis*, pages 1–11. IEEE, 2010.
- [67] S. J. Ruuth and B. Merriman. A simple embedding method for solving partial differential equations on surfaces. *J. Comput. Phys.*, 227(3):1943–1961, 2008.
- [68] Y. Saad and M. H. Schultz. GMRES: A generalized minimal residual algorithm for solving nonsymmetric linear systems. *SIAM J. Sci. Stat. Comput.*, 7(3):856–869, 1986.
- [69] B. Vallet and B. Lévy. Spectral Geometry Processing with Manifold Harmonics. *Computer Graphics Forum*, 27(2):251–260, 2008.
- [70] S. K. Veerapaneni, A. Rahimian, G. Biros, and D. Zorin. A fast algorithm for simulating vesicle flows in three dimensions. *J. Comput. Phys.*, 230(14):5610–5634, 2011.
- [71] B. Violeanu and V. Rokhlin. Spectra of Multiplication Operators as a Numerical Tool. *SIAM J. Sci. Comput.*, 36(1):A267–A288, 2014.
- [72] M. Wang, S. Leung, and H. Zhao. Modified Virtual Grid Difference for Discretizing the Laplace–Beltrami Operator on Point Clouds. *SIAM J. Sci. Comput.*, 40(1):A1–A21, 2018.
- [73] F. W. Warner. *Foundations of Differentiable Manifolds and Lie Groups*. Springer, New York, NY, 2013.
- [74] X. Xing and E. Chow. Interpolative decomposition via proxy points for kernel matrices. *SIAM J. Matrix Anal. Appl.*, 41(1):221–243, 2020.
- [75] L. Ying, G. Biros, and D. Zorin. A kernel-independent adaptive fast multipole algorithm in two and three dimensions. *J. Comput. Phys.*, 196(2):591–626, 2004.